

สถานะที่อุณหภูมิจำกัดของแอนติเฟอร์โรแมกเนตแบบฟรัสเทรตสองมิติ



นายมาฉิต แก้วทงศ์

สถาบันวิทยบริการ
จุฬาลงกรณ์มหาวิทยาลัย

วิทยานิพนธ์นี้เป็นส่วนหนึ่งของการศึกษาตามหลักสูตรปริญญาวิทยาศาสตรมหาบัณฑิต

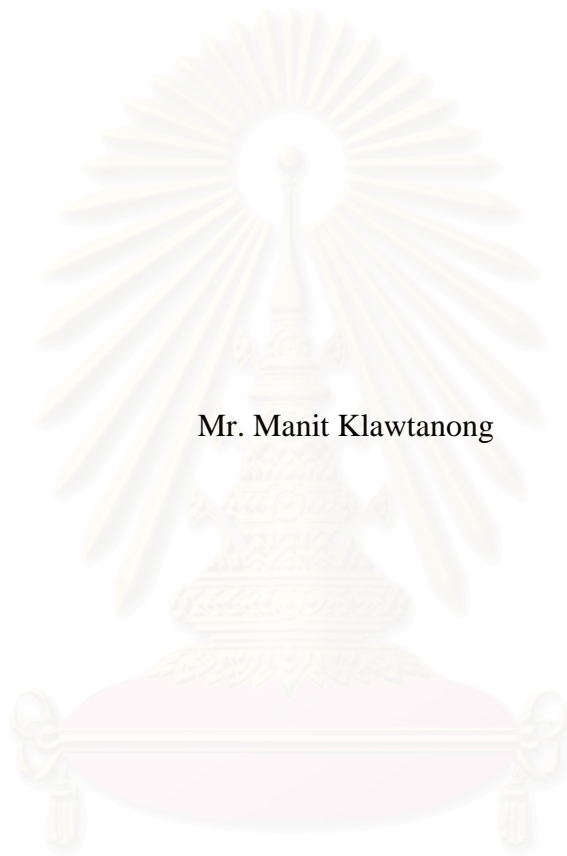
สาขาวิชาฟิสิกส์ ภาควิชาฟิสิกส์

คณะวิทยาศาสตร์ จุฬาลงกรณ์มหาวิทยาลัย

ปีการศึกษา ๒๕๕๑

ลิขสิทธิ์ของจุฬาลงกรณ์มหาวิทยาลัย

FINITE-TEMPERATURE STATES OF A TWO-DIMENSIONAL FRUSTRATED
ANTIFERROMAGNET



Mr. Manit Klawtanong

สถาบันวิทยบริการ
จุฬาลงกรณ์มหาวิทยาลัย

A Thesis Submitted in Partial Fulfillment of the Requirements
for the Degree of Master of Science Program in Physics

Department of Physics

Faculty of Science


Chulalongkorn University

Academic Year 2008


Copyright of Chulalongkorn University

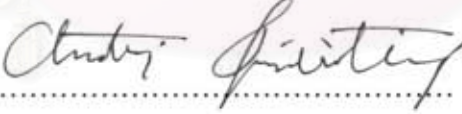
Thesis Title FINITE-TEMPERATURE STATES OF A TWO-DIMENSIONAL
FRUSTRATED ANTIFERROMAGNET
By Mr. Manit Klawtanong
Field of Study Physics
Advisor Chatchai Srinitiwarawong, Ph.D.

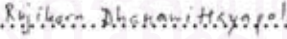
Accepted by the Faculty of Science, Chulalongkorn University in Partial
Fulfillment of the Requirements for the Master's Degree

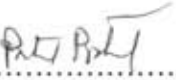

..... Dean of the Faculty of Science
(Professor Supot Hannongbua, Ph.D.)

THESIS COMMITTEE


..... Chairman
(Associate Professor Mayuree Natenapit, Ph.D.)


..... Advisor
(Chatchai Srinitiwarawong, Ph.D.)


..... Examiner
(Rujikorn Dhanawittayapol, Ph.D.)


..... External Examiner
(Assistant Professor Patcharee Pratumpong, Ph.D.)

มาฉิต แก้วทองคำ : สถานะที่อุณหภูมิจำกัดของแอนติเฟอร์โรแมกเนตแบบฟรัสเทรตสองมิติ. (FINITE-TEMPERATURE STATES OF A TWO-DIMENSIONAL FRUSTRATED ANTIFERROMAGNET) อ.ที่ปรึกษา
วิทยานิพนธ์หลัก : ดร. ฉัตรชัย ศรีนิตวรวงศ์, ๗๕ หน้า.

แบบจำลองเอกซ์วายของแอนติเฟอร์โรแมกเนตแบบฟรัสเทรตบนแลตทิซสามเหลี่ยมนี้เป็นแบบจำลองอย่างง่ายซึ่งอธิบายปรากฏการณ์วิกฤติของระบบแม่เหล็ก โดยเราได้ศึกษาการเปลี่ยนเฟสที่อุณหภูมิวิกฤติและบริเวณที่ใกล้กับอุณหภูมิวิกฤติโดยใช้ระเบียบวิธีจำลองแบบมอนติคาร์โลร่วมกับขั้นตอนวิธีแบบเมโทรโพลิซิส เพื่อที่จะให้ได้รูปแบบที่เป็นสเกลลิงของตัวแปรต่างๆ ผลกระทบของขนาดของระบบจะต้องนำมาพิจารณาด้วย ซึ่งผลที่ได้แสดงให้เห็นอย่างชัดเจนว่าการสูญเสียสมมาตรทั้งสองแบบนั้นเกิดขึ้นที่อุณหภูมิที่ต่างกัน คืออุณหภูมิคอสมอเตอร์ลิซซ์เทเลสส์กับอุณหภูมิไอซิงก์ อย่างไรก็ตามอุณหภูมิทั้งสองอยู่ห่างกัน 0.6 เเปอร์เซ็นต์เมื่อเทียบกับอุณหภูมิที่ต่ำกว่า ที่อุณหภูมิไอซิงก์การสูญเสียสมมาตรแบบสะท้อนได้เกิดขึ้นและเป็นไปตามการเปลี่ยนเฟสที่มีลักษณะคล้ายกับไอซิงก์ ขณะที่อุณหภูมิที่ต่ำกว่าอุณหภูมิไอซิงก์การสูญเสียสมมาตรแบบหมุนได้เกิดขึ้นและเป็นไปตามการเปลี่ยนเฟสแบบคอสมอเตอร์ลิซซ์เทเลสส์ นอกจากนี้เราพบลักษณะที่เป็นสเกลลิงของระยะความสัมพันธ์ของระบบไอซิงก์ โดยมีเลขชี้กำลังวิกฤติของตัวแปรดังกล่าวเท่ากับ 0.74 เมื่อพิจารณาผลของขนาดของระบบ ค่านี้จะลู่เข้า 0.83 ซึ่งต่างจากค่าของไอซิงก์ที่มีค่าเท่ากับ 1 ดูเหมือนว่าการเปลี่ยนเฟสที่มีลักษณะคล้ายกับไอซิงก์นั้นไม่ได้มีคุณสมบัติสากลที่เป็นไปตามการเปลี่ยนเฟสแบบไอซิงก์

ตัวแปรอื่นๆ เช่น พลังงานของระบบ ตัวแปรควบคุม ความจุความร้อนจำเพาะ สภาพรีบไว้ได้ทางแม่เหล็ก และฟังก์ชันความสัมพันธ์ที่บริเวณใกล้อุณหภูมิวิกฤติและที่บริเวณอุณหภูมิวิกฤติได้ถูกคำนวณและศึกษาเช่นเดียวกัน

ภาควิชา ฟิสิกส์
สาขาวิชา ฟิสิกส์
ปีการศึกษา ๒๕๕๑

ลายมือชื่อนิสิต วาณี / 11 กรกฎาคม ๖๐
ลายมือชื่ออ.ที่ปรึกษาวิทยานิพนธ์หลัก พิศาล ๗๗

4972441923 : MAJOR PHYSICS

KEYWORDS : ANTIFERROMAGNET / MONTE-CARLO / FRUSTRATED
MODEL / METROPOLIS ALGORITHM / CRITICAL TEMPERATURE

MANIT KLAWTANONG : FINITE-TEMPERATURE STATES OF A
TWO-DIMENSIONAL FRUSTRATED ANTIFERROMAGNET.

ADVISOR : CHATCHAI SRINITIWARAWONG, Ph.D., 75 pp.

The frustrated antiferromagnetic XY model on the triangular lattice is a simple model describing the critical phenomena of magnetic systems. By using the Monte Carlo simulation method associated with the Metropolis algorithm, we investigate phase transitions of the system at critical temperatures and near critical temperatures. To achieve a scaling form of important parameters, the finite size effect must be taken into account. Our results show clearly that the broken symmetries of the system occur at two separate critical temperatures, the Kosterlitz-Thouless temperature and the Ising-like temperature (T_I). However these temperatures lie close to each other about 0.6% compared with the lower temperature. At T_I , the reflection symmetry breaking transition occurs and it is known as the Ising-like transition. While at the lower temperature, the rotational symmetry breaking transition occurs and it is known as the Kosterlitz-Thouless transition. Moreover, we found the asymptotic behavior of the correlation length of the Ising-like transition with the critical exponent, $\nu = 0.74$. Taken into account the finite size effect, this value approaches 0.83 which differs from the value, $\nu = 1$, for the Ising universality class. It is likely that the Ising-like transition may not belong to the Ising universality class.

Also the other parameters such as the energy of the system, the order parameters, the specific heat, the magnetic susceptibility and the correlation functions have been calculated and their properties near the critical temperatures and at the critical temperatures have been studied.

Department : Physics
Field of Study : Physics
Academic Year : 2008

Student's Signature *Manit Klautanong*
Advisor's Signature *Chatchai Srinitiwara Wong*

Acknowledgements

I would like to express my sincere thanks to Dr. Chatchai Srinitiwara Wong, from whom I have got a chance to work in this field. I really appreciate all his suggestions and encouragement during this study. I would like to thank Dr. Varagorn Hengpunya for his suggestions about simulation techniques.

I would like to thank Assoc. Prof. Dr. Mayuree Natenapit, Dr. Rujikorn Dhanawittayapol and Asst. Prof. Dr. Patcharee Pratumpong who are on this thesis committee. I really appreciate their suggestions and comments.

I would like to thank the academics and all the members of the Semiconductor Physics Research Laboratory (SPRL) group, especially Asst. Prof. Dr. Sojiphong Chatraphon for the high efficiency and well organized workstation.

A lot of thanks go to all my friends. I have had enjoyable time with them. I want to thank Jureeporn Noodam who stands beside me and always cheers me up.

This thesis has been partially supported by Teaching Assistant Grant, Graduate School, Chulalongkorn University and the computations of this work have been partially done using the Computer Cluster at the Computer Center, Faculty of Science, Chulalongkorn University.

Last but not least, I would like to thank my family, my mother who is everything for me, my father, my brother, my sister and all relatives who give me not only love but also financial support. My life is meaningless without them.

จุฬาลงกรณ์มหาวิทยาลัย

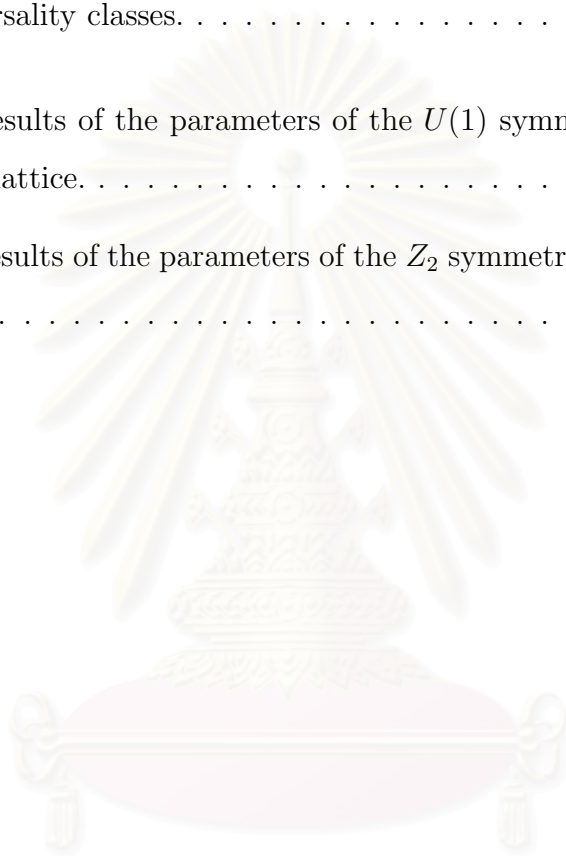
Contents

Abstract (Thai)	iv
Abstract (English).....	v
Acknowledgements.....	vi
Contents	vii
List of Tables.....	ix
List of Figures.....	x
1 Introduction.....	1
2 Theoretical Aspects	3
2.1 Phase transitions	3
2.2 The <i>FAXY</i> model	6
2.2.1 Frustration	8
2.3 Thermodynamic parameters	10
2.4 Critical phenomena	13
2.4.1 The $U(1)$ symmetry breaking transition	14
2.4.2 The Z_2 symmetry breaking transition	15
2.4.3 Universality classes	16
3 Simulation methods	18
3.1 The Metropolis algorithm	19

4	Results and Discussions	22
4.1	The spin and the staggered chirality configurations	24
4.2	Critical temperatures	27
4.2.1	The Kosterlitz–Thouless transition temperature	27
4.2.2	The Ising–like transition temperature	27
4.3	The energy of the system	30
4.4	Order parameters	32
4.4.1	The sublattice magnetization	32
4.4.2	The staggered chirality	35
4.5	The specific heat	38
4.6	The magnetic susceptibility	45
4.7	Correlation functions	48
4.7.1	The spin–spin correlation function	48
4.7.2	The chirality–chirality correlation function	52
4.8	Correlation lengths	56
4.8.1	The correlation length of spins	56
4.8.2	The correlation length of chirality	59
5	Conclusions	64
	References	67
	Appendices	72
	Appendix A : Finite Size Scaling	72
	Appendix B : Cumulants	73
	Vitae	75

List of Tables

2.1	The behavior of the order parameters for the $U(1)$ and the Z_2 symmetries.	17
2.2	Universality classes.	17
4.1	The results of the parameters of the $U(1)$ symmetry on the triangular lattice.	63
4.2	The results of the parameters of the Z_2 symmetry on the triangular lattice.	63



สถาบันวิทยบริการ
จุฬาลงกรณ์มหาวิทยาลัย

List of Figures

2.1	A simple phase diagram of a ferromagnet (a), the field dependence of the free energy and its derivatives (b), (c) and (d), and the temperature dependence of its derivatives (e) and (f).	5
2.2	The <i>FAXY</i> model on a triangular lattice of $L = 6 \times 6$ lattice sites. The arrows represent spins and the colors represent spins in sublattices <i>A</i> , <i>B</i> and <i>C</i>	7
2.3	A low temperature state of non-frustrated spin models (a), (b) and (c), and the frustrated spin model (d).	9
2.4	The shaded triangles refer to triangles <i>i</i> , the up- and down- triangles <i>i</i> are denoted by Δ_i and ∇_i	11
3.1	A flow chart of our simulation in the <i>FAXY</i> model.	21
4.1	The time evolution of the energy of 12×12 lattice sites at the temperature, $T = 0.510$, the equilibrium time of the system is approximately 600 MCSs which is marked by the dash line.	23
4.2	The spin configurations of $L = 240 \times 240$ at different temperatures, the colors represent the angles of the spins respected to an arbitrary direction.	25
4.3	The staggered chirality configurations of $L = 240 \times 240$ at different temperatures, the colors represent the values of the staggered chirality.	26
4.4	The Binder cumulant for the magnetization is plotted against the temperature at different system sizes. The dash line marks the critical temperature $T_{KT} = 0.509(8)$	28

4.5	The Binder cumulant for the staggered chirality is plotted against the temperature at different system sizes. The dash line marks the critical temperature $T_I = 0.513(0)$	29
4.6	The energy of the system is plotted against the temperature at different system sizes.	31
4.7	The sublattice magnetization is plotted against the temperature at different system sizes.	33
4.8	The sublattice magnetization near the critical temperature $T \leq T_{KT}$ is plotted against the system size at different temperatures. The dash line has a slope -0.16 at $T = T_{KT}$	34
4.9	The staggered chirality is plotted against the temperature at different system sizes.	36
4.10	The staggered chirality is plotted against the reduced temperature at different system sizes. The dash line has a slope $= 0.125$	37
4.11	The specific heat is plotted against the temperature at different system sizes.	39
4.12	The specific heat is plotted against the reduced temperature at different system sizes. The dash line has a slope $= -0.45$	41
4.13	The specific heat is plotted against the reduced temperature at different system sizes.	42
4.14	The peak of the specific heat at different system sizes is plotted against the system size, (a) the dash line indicates $\alpha/\nu = 0.52$ and (b) the dash line indicates $\alpha/\nu = 0$	43
4.15	The magnetic susceptibility is plotted against the temperature at different system sizes.	46
4.16	The magnetic susceptibility is plotted against the reduced temperature at different system sizes, the dash line has a slope -1.05 and the solid line has a slope -1.23	47

4.17	The correlation function C_m is plotted against the distance at the critical temperature T_{KT}	49
4.18	The correlation function C_m is plotted against the distance at the critical temperature T_{KT} . The dash line has a slope = -0.30	50
4.19	The system size dependence of η_{KT} is plotted against the inverted system size $1/L$. The dash line marks the actual value of $\eta_{KT} = 0.25$	51
4.20	The correlation function C_h is plotted against the distance at the critical temperature T_I	53
4.21	The correlation function C_h is plotted against the distance at the critical temperature T_I . The dash line has a slope = -0.19	54
4.22	The system size dependence of η_I is plotted against the inverted system size $1/L$. The dash line marks the actual value of $\eta_I = 0.25$	55
4.23	The correlation length ξ_m is plotted against the reduced temperature at different system sizes.	57
4.24	The correlation length ξ_m is plotted against the reduced temperature at different system sizes, the solid line denotes an exponential decay as $\xi_m = 2.50\exp(0.19t^{-1/2})$	58
4.25	The correlation length ξ_h is plotted against the reduced temperature at different system sizes.	60
4.26	The correlation length ξ_h is plotted against the reduced temperature at different system sizes. The dash line has a slope = -0.74	61
4.27	The system size dependence of ν is plotted against the inverted system size $1/L$. The dash line marks the value $\nu = 0.83$	62

CHAPTER I

Introduction

Frustrated two-dimensional spin models have been the subjects of interest in condensed matter physics. They play an important role in the study of phase transitions in a wide range of physical systems. Some interesting models in the last two decades are the fully frustrated XY ($FFXY$) model [1–15] and the frustrated antiferromagnetic XY ($FAXY$) model [5, 14, 20–23]. These models describe an array of Josephson junctions under an external magnetic field [2, 16] and discotic liquid crystals [17]. Another version of frustrated models is the frustrated antiferromagnetic six-state clock model which describes the orientational ordering of CF_3Br monolayers physisorbed on graphite [18, 19].

The frustrated models have a continuous $U(1)$ symmetry as a non-frustrated XY model [25] and an additional discrete reflection Z_2 symmetry or a chiral symmetry as the Ising model. These symmetries can be broken at critical temperatures through the Kosterlitz–Thouless (KT) transition and an Ising-like transition, respectively. The existence of this additional Z_2 symmetry due to the chirality of the system induces degenerate states of the system and complex structures at low temperatures.

There are two important questions for the nature of the frustrated system. First, the KT transition and the Ising-like transition occur at the same critical temperature or at two separate critical temperatures. Second, the Ising-like symmetry breaking transition belongs to the Ising universality class or a non-Ising universality class. Since, a lot of results from both theoretical and simulation studies in these models [2–15, 18–23, 26–28] have had no consensus. Some re-

sults show that two symmetry breaking transitions occurred at a single transition temperature [3–5, 13, 21] depending on some parameters [4, 7]. Moreover, the Ising–like transition was found that it may not belong to the Ising universality class [5–9, 11–15, 19, 22, 26, 27].

On the other hand, two separate transition temperatures were found [6, 9–11, 14, 15, 18, 19, 22, 27, 28], the KT transition occurs slightly lower than the Ising–like transition, $T_{KT} < T_I$. Furthermore, the Ising behavior was also found [2], the asymptotic behavior of the specific heat followed the logarithmic behavior rather than a power law decay which was found in those models. This behavior appears when a system size is greater than a critical system size [18] corresponding with the Olsson’s argument [10].

In this thesis, we investigate phase transitions of the frustrated antiferromagnetic XY ($FAXY$) model on a triangular lattice. By using the Monte Carlo simulation method associated with the Metropolis algorithm, we study the behavior of the frustrated system at the critical temperatures and near the critical temperatures. This thesis is organized as follows. Chapter 2, we provide background knowledge and related theory about the spin system. In Chapter 3, we will give the simulation details of this work. Our results are shown in Chapter 4. Also, the inconsistency in the behavior of the frustrated system will be discussed in this Chapter. Finally, our results will be concluded in Chapter 5.

CHAPTER II

Theoretical Aspects

2.1 Phase transitions

In physical systems, phase transitions can be predicted by the thermodynamic potential such as the free energy. It occurs when there is a singularity in the free energy or one of its derivatives. If the first derivatives of the free energy, for example, the order parameter, are discontinuous at the critical temperature T_c , the transition is termed first order. The most common example corresponding to this transition is a liquid–solid transition which has a discontinuous change in the density which is the order parameter of the system.

For second order phase transitions, if the first derivatives are continuous but second derivatives are discontinuous or infinite, the transition will be described as a higher order, second order or critical. This type of the transition corresponds to a divergence of the susceptibility, an infinite correlation length, and a power law decay of correlation functions. In the magnetic system with a zero external field, it refers to the magnetization which varies continuously from zero in a disordered state (paramagnet) to a finite value in an ordered state (ferromagnet or antiferromagnet) through the critical temperature. At this temperature, the specific heat and the magnetic susceptibility also approach infinity. The order parameter which plays an important role of a phase transition must separate the order phase from the disorder phase, so it will be defined consistently. The order parameter is defined differently in different kinds of physical systems. In a magnetic system it indicates the spontaneous magnetization [29].

To illustrate the idea of phase transitions, we use a simple ferromagnet in presence of the magnetic field. In figure 2.1(a) shows the phase diagram of this system, there is a line of the first–order transition along $H = 0$ which ends at a critical point at $T = T_c$. The broken lines 1 ($T < T_c$), 2 ($T = T_c$) and 3 ($T > T_c$) represent the field dependence of the free energy and its field derivatives, the magnetization and the susceptibility, at constant temperatures. The lines 4 ($H > 0$), 5 ($H = 0$) and 6 ($H < 0$) represent the temperature dependence of those parameters at the constant field. The free energy of the system is shown in figure 2.1(b), it is symmetric about $H = 0$. For $T < T_c$, there is a signal of discontinuity of its derivative, the magnetization M , respected to the field at $H = 0$. Clearly, in figure 2.1(c), the magnetization becomes discontinuous at $H = 0$ for $T < T_c$, but for $T > T_c$, it varies continuously. At $T = T_c$, the magnetization has a continuous change; however, it has an infinite slope associated with the divergence of the susceptibility at $H = 0$. Next, the isothermal susceptibility χ_T , which is the first derivative of the magnetization respected to the field, is shown in figure 2.1(d). For $T \neq T_c$, the finite susceptibility varies continuously, but for $T = T_c$, the susceptibility diverges at $H = 0$. It corresponds to the second–order phase transition at $H = 0$.

Note that, it only has first– and second–order phase transitions when the system passes along path 5 which has the zero field. The figure 2.1(e) and 2.1(f) show variations of the magnetization and the susceptibility with the temperature at the constant field referring to path 4, 5 and 6. The temperature dependence of the magnetization is shown in figure 2.1(e). For $H \neq 0$, the magnetization increases smoothly with decreasing the temperature and approaches to its saturation value at $T = 0$, in which all spins align in the direction of the field. If $H > 0$, the magnetization is positive and vice versa. For $H = 0$ and $T > T_c$, the spins align in both directions equally, up and down, so it has the zero magnetization in this region. At the critical temperature, the correlation length becomes infinity, so an infinitely small field can induce the spins to align in the only one direction. The magnetization increases from zero at $T = T_c$ to a finite value below T_c and

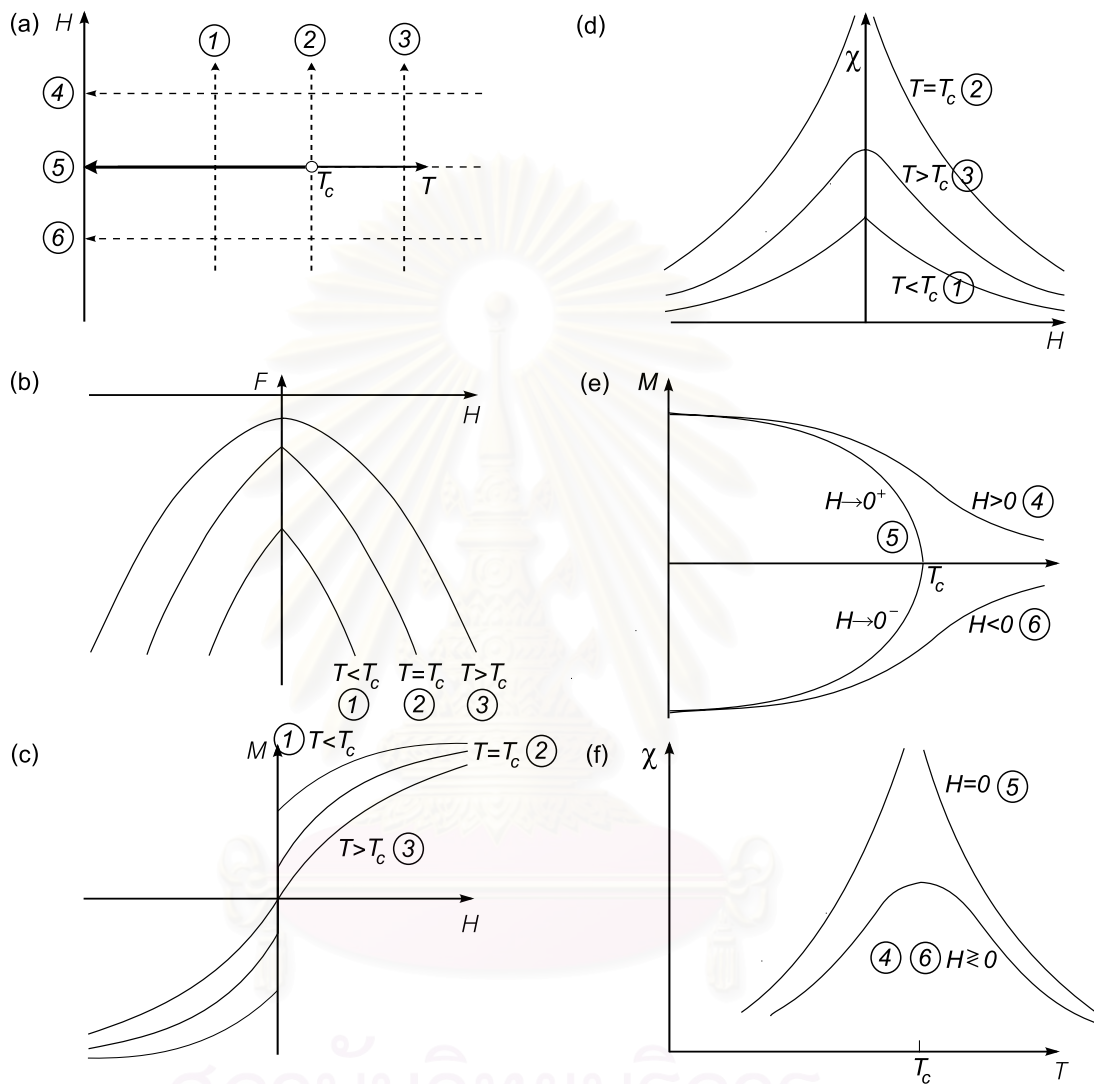


Figure 2.1: A simple phase diagram of a ferromagnet (a), the field dependence of the free energy and its derivatives (b), (c) and (d), and the temperature dependence of its derivatives (e) and (f).

approaches to its saturation value at $T = 0$. The final state of the magnetization depends on an infinitely small field at $T = T_c$. The positive magnetization corresponds to a positive field and vice versa.

Finally, the temperature dependence of the susceptibility is shown in figure 2.1(f). For $H \neq 0$, the susceptibility varies continuously at all temperatures and it has a peak at $T = T_c$. For $H = 0$, the peak of the susceptibility at $T = T_c$ becomes infinity due to the infinite slope of the magnetization at $T = T_c$ as shown in figure 2.1(e).

According to a study of phase transitions, the most studied subject is how the system behaves near the critical temperature or at the critical temperature. Interestingly, when the temperature is near the critical temperature the thermodynamic functions can be usually described as some power law which can be written as

$$F(t) \sim t^\lambda, \quad (2.1)$$

when $F(t)$ is a thermodynamic function, λ is a critical exponent and $t = (T - T_c)/T_c$ is a reduced temperature which plays a central role of the temperature. The \sim sign in Eq. (2.1) only represents the asymptotic behavior of the function $F(t)$ as $t \rightarrow 0$ [29]. This behavior will be described later in the next section.

2.2 The *FAXY* model

We investigate phase transitions of the frustrated antiferromagnetic *XY(FAXY)* model on a triangular lattice. This model is expected to have the same behavior as the *FFXY* model on the square lattice [24]. It has a continuous $U(1)$ symmetry and an additional discrete Z_2 symmetry corresponding to the spins and the staggered chirality, respectively. The *FAXY* model is shown in figure 2.2, each spin lies on a lattice site with six-nearest neighbor spins and it can rotate continuously on the plane. The magnitude of the spins is a constant which usually equals to one. The arrow heads represent the spin directions and the color cycles refer to

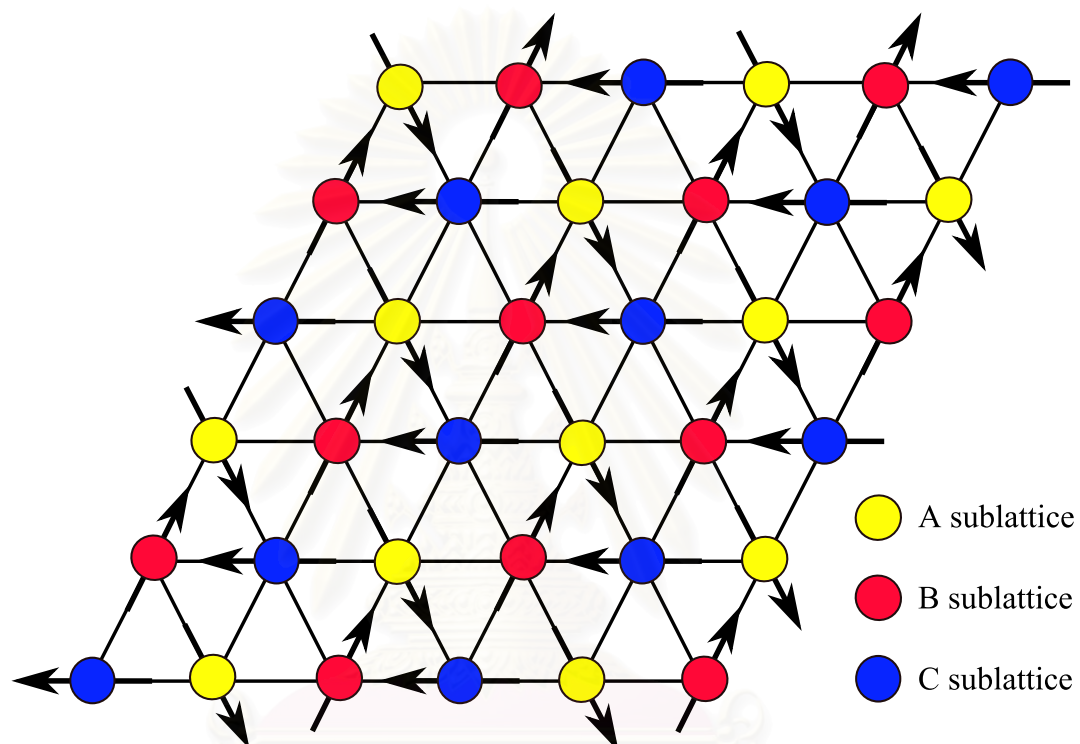


Figure 2.2: The *FAXY* model on a triangular lattice of $L = 6 \times 6$ lattice sites. The arrows represent spins and the colors represent spins in sublattices *A*, *B* and *C*.

สถาบันวิทยบริการ
จุฬาลงกรณ์มหาวิทยาลัย

the spins in sublattice sites. We divide the lattice into three sublattices because this system requires that the net magnetization is canceled both above and below the critical temperature. However, the nature of the order of the system in both regions is different. Above the critical temperature the spins lie in all directions randomly, so the system is said to be a disordered state. While, at below the critical temperature the spins can lie in some directions, then the system is said to be an ordered state. For this reason, we also use the magnetization of one of these sublattices to define order parameters which indicate the order of the system. Note that, the spin configuration in the figure only appears in a ground state due to the spins in the same sublattice align in the same direction. The Hamiltonian of the system in a zero field can be written as

$$H = -J \sum_{\langle i,j \rangle} \vec{S}_i \cdot \vec{S}_j, \quad (2.2)$$

when J is the exchange energy. It is negative for antiferromagnet and positive for ferromagnet. We shall use $\langle i,j \rangle$ to denote a sum over nearest neighbor spins. The spin \vec{S}_i is a classical spin variable and it has a continuous rotation on that plane. Eq. (2.2) can be written as

$$H = -J \sum_{\langle i,j \rangle} \cos(\theta_i - \theta_j), \quad (2.3)$$

when $|\vec{S}_i|$ equals to one. Here θ_i is an angle of spin i respected to an arbitrary direction lying on that plane. The Hamiltonian of the system in Eq. (2.3) only depends on the angle between the spins, so the Hamiltonian of the system is invariant under the rotation.

2.2.1 Frustration

Normally, spins lie themselves in a direction which provides the minimum energy. For example, the two-dimensional Ising model on the square lattice, spins lie in the same direction for a ferromagnet and lie in the antiparallel direction against nearest neighbor spins for an antiferromagnet. However, there are some models

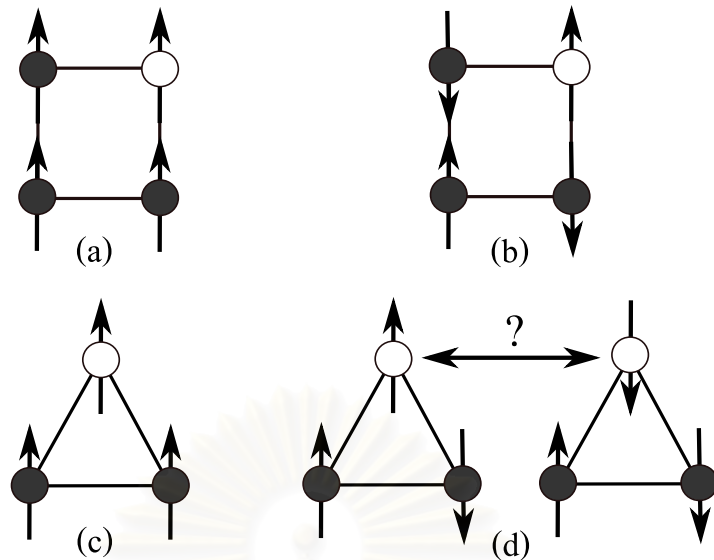


Figure 2.3: A low temperature state of non-frustrated spin models (a), (b) and (c), and the frustrated spin model (d).

that have degenerate states corresponding to shapes of lattices and the exchange energy of the system. One of these models is the *FAXY* model which has degenerate states at low temperatures. It means that some spins have more than one possibility of choosing their positions. The states which have the same minimum energy are identical for the spins, so these models are called frustrated models and this characteristic is called ‘frustration.’

To illustrate the frustration, we use the *FAXY* model compared to non-frustrated models as shown in figure 2.3. In figure 2.3(a) and 2.3(b) show the ferromagnetic and antiferromagnetic models on the square lattice, respectively. While in figure 2.3(c) and 2.3(d) show the ferromagnetic and antiferromagnetic models on the triangular lattice. Clearly, in the figure 2.3(a), 2.3(b) and 2.3(c) are the non-frustrated models whereas in the figure 2.3(d) is a frustrated model. For the non-frustrated models, when the dark color spins align in the directions as shown in the picture, the light color spins have the only one direction corresponding to the minimum energy of the state. But for the frustrated model or in the figure 2.3(d), if directions of the dark color spins align in the directions, the light color

spin can lie in two directions which have the same minimum energy. This behavior directly affects the spin configurations and it also creates complex structures at low temperature states.

2.3 Thermodynamic parameters

For a system is in an equilibrium state, the essential information is kept in a partition function. The general form of the partition function for a classical system is written as [29, 30]

$$Z = \sum_{\mu} e^{-E_{\mu}/k_B T}, \quad (2.4)$$

when E_{μ} is the energy of state μ , T is the temperature and k_B is the Boltzmann constant. The sum in Eq. (2.4) is over all possible states of the system and it depends on the size of the system and the number of degrees of freedom for each particle. The probability of the system occupying any particular state is also determined by the partition function. Therefore the probability that the system is in state μ is given by

$$P_{\mu} = \frac{1}{Z} e^{-E_{\mu}/k_B T}. \quad (2.5)$$

The average of a given thermodynamic parameter A can be written as the sum over all microstates in phase space and weighted according to Eq. (2.5) as

$$\langle A \rangle = \frac{1}{Z} \sum_{\mu} A_{\mu} e^{-E_{\mu}/k_B T} = \sum_{\mu} P_{\mu} A_{\mu}. \quad (2.6)$$

The first thermodynamic parameter is the energy of the system which can be written as

$$\langle e \rangle = \frac{1}{N} \langle E \rangle, \quad (2.7)$$

where N is the total spin in the system and $\langle \dots \rangle$ sign denotes an average over all states. Note that, the energy of the system in Eq. (2.7), actually, is the energy per spin. The order parameter of the system is the sublattice magnetization which is given by

$$\langle m_A \rangle = \frac{3}{N} \langle M_A \rangle, \quad (2.8)$$

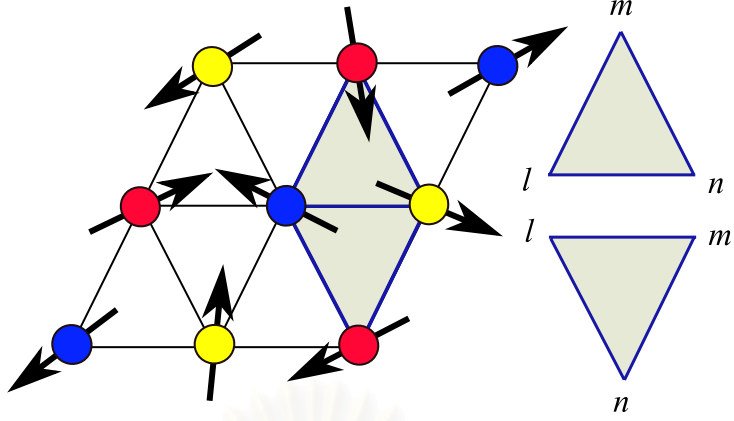


Figure 2.4: The shaded triangles refer to triangles i , the up- and down- triangles i are denoted by \triangle_i and ∇_i .

when M_A is the net magnetization in A sublattice defined by

$$M_A = \left| \sum_{i \in A} \vec{S}_i \right|, \quad (2.9)$$

where the sum runs only over the sites in the A sublattice, also $\langle m_B \rangle$ and $\langle m_C \rangle$ are defined analogously. Although the magnetization is a vector quantity we are only interested in the magnitude of the magnetization to indicate the spontaneous symmetry breaking. The $\langle m_A \rangle$ plays a role of the order parameter for the $U(1)$ symmetry breaking transition. For the $FAXY$ model, the system has an additional Z_2 symmetry, so it is necessary to define the order parameter to indicate the Z_2 spontaneous symmetry breaking. The order parameter can be defined by using the chirality of each elementary triangle which is written as

$$h_{\triangle_i, \nabla_i} = \frac{2}{3\sqrt{3}} [\sin(\theta_m - \theta_l) + \sin(\theta_n - \theta_m) + \sin(\theta_l - \theta_n)], \quad (2.10)$$

where \triangle_i and ∇_i denote up- and down-triangles i as shown in figure 2.4, and h_{\triangle_i} is the chirality of up-triangle i . If we look at the up-triangle i , the indexes l , m and n in Eq. (2.10) refer to spins l , m and n for the chirality of up-triangle i . The chirality of down-triangle i can be defined in the same manner. The θ_l is the angle of spin l respected to an arbitrary direction and it is different between up- and down-triangles. The order parameter for the Z_2 symmetry breaking transition is the staggered chirality, $\langle h \rangle$. The staggered chirality defined by the

chirality can be written as

$$\langle h \rangle = \frac{1}{2N} \left\langle \sum_i (h_{\Delta_i} - h_{\nabla_i}) \right\rangle. \quad (2.11)$$

The staggered chirality in Eq. (2.11) can be either positive (+1) or negative (-1) at the ground state and it also has the zero chirality at high temperature states.

The other interesting parameters related to the fluctuation of the energy and the magnetization are the specific heat and the isothermal susceptibility. The specific heat defined from the energy fluctuation relation is given by

$$c_V = \frac{N}{k_B T^2} (\langle e^2 \rangle - \langle e \rangle^2). \quad (2.12)$$

The magnetic susceptibility from the magnetization fluctuation relation is also defined in the same manner as

$$\chi = \frac{N}{k_B T} (\langle m_A^2 \rangle - \langle m_A \rangle^2). \quad (2.13)$$

To determine the critical temperatures, we use the Binder cumulants or the reduced fourth order cumulants [31, 32] defined by

$$B_m = 1 - \frac{\langle m_A^4 \rangle}{3 \langle m_A^2 \rangle^2}, \quad (2.14)$$

$$B_h = 1 - \frac{\langle h^4 \rangle}{3 \langle h^2 \rangle^2}. \quad (2.15)$$

B_m is the Binder cumulant that can be used to identify $U(1)$ symmetry breaking transition for the magnetization and B_h is the Binder cumulant that can be used to identify Z_2 symmetry breaking transition for the chirality. These quantities are obtained by considering the probability distributions of the order parameters in higher orders of cumulants (see Appendix B). The Binder cumulants depend on the system sizes and temperatures both above and below the critical temperatures. But at critical points, the Binder cumulants are independent of the system sizes, and then the critical temperatures will be determined by the crossing points of them.

Although, those thermodynamic parameters defined earlier have been used to describe the macroscopic properties, we are also interested in the microscopic properties. To obtain any microscopic properties, the correlation functions will be considered. We find the spin–spin correlation function and the chirality–chirality correlation function of up–triangles in the vertical direction to determine the universality class of the system. The spin–spin correlation function is defined by

$$C_m(r) = \frac{3}{N} \left\langle \sum_{i \in A} \cos(\theta_i - \theta_{i+r}) \right\rangle, \quad (2.16)$$

when $i + r$ denotes a position of a site displaced by the distance r in the vertical direction from site i . For *FAXY* model, the distance r is limited to the maximum distance, $r_{max} = L/4$, in the vertical direction. The chirality–chirality correlation function is defined by

$$C_h(r) = \frac{3}{N} \left\langle \sum_{i \in A} h_{\Delta_i} h_{\Delta_{i+r}} \right\rangle, \quad (2.17)$$

when Δ_i denotes up–triangle i (see figure 2.4). Moreover, to indicate a critical state we use the correlation lengths which can be defined by using the correlation functions. The correlation lengths are given by

$$\xi_m = \left[\sum_r r^2 C_m(r) / \sum_r C_m(r) \right]^{1/2}, \quad (2.18)$$

$$\xi_h = \left[\sum_r r^2 C_h(r) / \sum_r C_h(r) \right]^{1/2}, \quad (2.19)$$

for the magnetization and the chirality, respectively [18].

2.4 Critical phenomena

The term critical phenomena refers to the thermodynamic properties of systems near the critical temperature of a second–order phase transition. The behavior of these thermodynamic parameters depends on some details of a given system such as the dimension or the degree of freedom of the order parameter which corresponds to the symmetry of the system. For the *FAXY* model, the degrees

of freedom of the spin and the staggered chirality correspond to the $U(1)$ and Z_2 symmetries. The critical behavior of thermodynamic parameters is described below [30].

2.4.1 The $U(1)$ symmetry breaking transition

An unusual phase transition in two dimensions is the KT phase transition. The magnetic susceptibility is found to be a finite value at a disordered state at high temperatures and an infinite value at a quasi-long range ordered state at low temperatures. The magnetic correlation length diverges faster than a power law of the critical behavior as $T \rightarrow T_{KT}^+$ and becomes infinity at a quasi-long range order state at $T \leq T_{KT}$. Although the correlation of the spin becomes zero when $r \rightarrow \infty$ both above and below the critical temperature, the asymptotic forms of the correlation function are different. At high temperatures, the magnetic correlation function decays exponentially. While at low temperatures, the magnetic correlation function decays as a power law

$$C_m(r) \sim \frac{e^{-r/\xi_m}}{r^{d-2+\eta_{KT}}} ; T > T_{KT}, \quad (2.20)$$

$$C_m(r) \sim \frac{1}{r^{d-2+\eta'_{KT}}} ; T \leq T_{KT}, \quad (2.21)$$

where d is the dimension of the system, η_{KT} is a critical exponent, η'_{KT} is the same critical exponent except it depends on temperatures and ξ_m is the correlation length which determines the size of the largest ordered clusters in the system. The universal value of the critical exponent $\eta'_{KT} = \eta_{KT} = \frac{1}{4}$ at $T = T_{KT}$ for the XY model. The power law decay of the magnetic correlation function indicates that the system is already set in the critical state. The magnetic correlation length decays exponentially at $T > T_{KT}$ and becomes infinity at $T \leq T_{KT}$

$$\xi_m \sim \exp(a_0 t^{-1/2}) ; T > T_{KT}, \quad (2.22)$$

$$\xi_m \longrightarrow \infty ; T \leq T_{KT}, \quad (2.23)$$

when $t = (T - T_{KT})/T_{KT}$ and a_0 is a constant. The specific heat and the magnetic susceptibility were also found to be an exponential decay at high temperature states and become infinity at $T \leq T_{KT}$ as a function of the correlation length

$$cV_m \sim \xi_m^{-d} \quad ; \quad T > T_{KT}, \quad (2.24)$$

$$\chi_m \sim \xi_m^{2-\eta_{KT}} \quad ; \quad T > T_{KT}. \quad (2.25)$$

The sublattice magnetization, actually, is zero at all temperatures in this model [25] but for a finite system size the sublattice magnetization depends on the system size at low temperatures as

$$m_A \sim L^{-x} \quad ; \quad T \leq T_{KT}, \quad (2.26)$$

where x is an exponent and it also depends on temperatures. This value equals to $1/8$ at the critical temperature. At high temperatures, the sublattice magnetization is still zero.

2.4.2 The Z_2 symmetry breaking transition

The chirality–chirality correlation function decays exponentially to zero with the distance between the up–triangles near the critical temperature both above and below the critical temperature and it becomes a power law at the critical temperature as

$$C_h(r) \sim \frac{e^{-r/\xi_h}}{r^{d-2+\eta_I}} - h^2 \quad ; \quad T \neq T_I, \quad (2.27)$$

$$C_h(r) \sim \frac{1}{r^{d-2+\eta_I}} \quad ; \quad T = T_I, \quad (2.28)$$

where η_I is a critical exponent, ξ_h is the correlation length and h^2 is a constant relating to the staggered chirality and it is zero at $T \geq T_I$. In the thermodynamic limit, the correlation length near the critical temperature is followed by

$$\xi_h \sim |t|^{-\nu} \quad ; \quad T \neq T_I, \quad (2.29)$$

$$\xi_h \rightarrow \infty \quad ; \quad T = T_I, \quad (2.30)$$

where $t = (T - T_I)/T_I$ and ν is a critical exponent. At the critical point, the correlation length becomes infinity so the correlation function decays as a power law. The other thermodynamic parameters, the susceptibility and the specific heat are given by

$$\chi_h \sim |t|^{-\gamma} \quad ; \quad T \neq T_I, \quad (2.31)$$

$$c_{V_h} \sim |t|^{-\alpha} \quad ; \quad T \neq T_I, \quad (2.32)$$

when γ and α are critical exponents. Also, the magnetic susceptibility and the specific heat diverge at the critical temperatures. Note that for the two-dimensional Ising model the specific heat diverges logarithmically, so the exponent $\alpha = 0$. The staggered chirality or the order parameter of the Z_2 symmetry breaking transition has asymptotic behavior near the critical point as

$$h \sim (-t)^\beta \quad ; \quad T < T_I, \quad (2.33)$$

when β is a critical exponent. Eq. (2.33) is only true where the temperature of the system is less than the critical temperature. Since the staggered chirality becomes zero at high temperatures, $T \geq T_I$ [29].

The two-dimensional behavior of all parameters of the $U(1)$ and the Z_2 symmetries at $T < T_C$, $T = T_C$ and $T > T_C$ is listed in Table 2.1.

2.4.3 Universality classes

In a critical region, systems only depend on a few fundamental parameters. For models with a short-range interaction these are the dimensionality of space, d , and the symmetry of the order parameter. Then any systems that have the same dimension and the symmetry of the order parameter, they must have the same critical exponents and belong to the same universality class. Usually, universality classes are labeled by the simplest model of the systems belonging to them. The critical exponents which are used to indicate the universality class of the system can be directly obtained by simulations. There are some universality classes and

critical exponents listed in Table 2.2 [29]. In the Table H refers to the field dependence of the magnetization along the critical isotherm ($T = T_C$), $H \sim |M|^\delta \text{sgn}(M)$, where the $\text{sgn}(x)$ is the signum function.

Table 2.1: The behavior of the order parameters for the $U(1)$ and the Z_2 symmetries.

Parameter	$U(1)$ symmetry		Z_2 symmetry		
	$T > T_{KT}$	$T \leq T_{KT}$	$T > T_I$	$T = T_I$	$T < T_I$
$C_{m, h}(r) \sim$	$\frac{e^{-r/\xi_m}}{r^{\eta_{KT}}}$	$\frac{1}{r^{\eta_{KT}}}$	$\frac{e^{-r/\xi_h}}{r^{\eta_I}}$	$\frac{1}{r^{\eta_I}}$	$\frac{e^{-r/\xi_h}}{r^{\eta_I}} - h^2$
$\xi_{m, h} \sim$	$\exp(a_0 t^{-1/2})$	∞	$ t ^{-\nu}$	∞	$ t ^{-\nu}$
$c_{V_{m, h}} \sim$	ξ_m^{-2}	∞	$ t ^{-\alpha}$	∞	$ t ^{-\alpha}$
$\chi_{m, h} \sim$	$\xi_m^{2-\eta_{KT}}$	∞	$ t ^{-\gamma}$	∞	$ t ^{-\gamma}$
$m_A, h \sim$	0	L^{-x}	0		$(-t)^\beta$

Table 2.2: Universality classes.

Universality class	c_V	m	χ	H	ξ	$C(r)$
	α	β	γ	δ	ν	η
2-d Ising	0(log)	1/8	7/4	15	1	1/4
3-d Ising	0.10	0.33	1.24	4.8	0.63	0.04
3-d XY	0.01	0.34	1.30	4.8	0.66	0.04
3-d Heisenberg	-0.12	0.36	1.39	4.8	0.71	0.04
mean field	0(dis.)	1/2	1	3	1/2	0
3-d Potts, $q = 3$,	1/3	1/9	13/9	14	5/6	4/15
$q = 4$	2/3	1/12	7/6	15	2/3	1/4

CHAPTER III

Simulation methods

In this work, we initially set the system at a high temperature state or at the ground state and then we decrease (increase) the temperature suddenly to a lower (higher) temperature state. After that, the system will be reached to a new equilibrium state. The evolution of the system will be followed a stochastic process rather than Newton's laws. When the system is in an equilibrium state it does not depend on time and then the thermodynamic parameters will fluctuate around some averaged value. To simulate the stochastic process it is necessary to use random numbers created from a computer. Random numbers which are created from a computer are not perfectly random and they are usually called the 'pseudo-random' numbers. The difference of the random number generators can also affect the equilibrium state, but it seems as a statistical error and it can be reduced by averaging the thermodynamic parameters over independent runs of the successive simulations and by increasing the system size. This procedure that uses the random numbers to create a stochastic process is called the Monte Carlo method. We use the random number generator (ran4) [33] to generate uniform random numbers in the interval $(0, 1)$. It is important that a random number generator must have good behavior corresponding to an appropriate system. For example, any sequential numbers should be uncorrelated, have a large period and a uniform distribution.

In this model, the periodic boundary conditions must be imposed to treat the 'edges' or boundaries of the lattice. This condition, the first spin can see the last spin in the same column as a neighbor spin and vice versa. The condition

is true for the spins in the same row. This procedure can eliminate the effect of the boundaries. But for a finite system the finite size effect still holds the characteristics of the system especially when the correlation length becomes infinity at a critical point. For our model, the maximum distance of the correlation functions is limited to $L/4$ in the vertical direction, so the resultant properties of the system will differ from the infinite system. Note that for the antiferromagnetic models, the order parameter is usually the sublattice magnetization, if we choose the system size incorrectly the sublattice mismatch of the spins will be occurred [31].

3.1 The Metropolis algorithm

We refer to Eq. (2.6) again. Unfortunately, because the configurations of the system are so huge and then we can not generate every all possible states in the system. For example, the Ising model on a lattice of N sites the sum is over 2^N configurations. This is a number which increases very quickly with N and a direct evaluation is feasible only $N \lesssim 40$. However, it is possible to choose the independent states in the region where they mostly contribute to average. This is called the importance sampling and then the average of A over n successive states converges to the thermodynamic average defined in Eq. (2.6)

$$\langle A \rangle_n = \langle A \rangle + O(n^{-1/2}). \quad (3.1)$$

In the limit $n \rightarrow \infty$ each state is weighted by its Boltzmann factor, $e^{-E/k_B T}$. For the previous reason, this is how we generate the desired states. For the stochastic models, the time-dependent behavior is described by a master equation

$$\frac{\partial P_n(t)}{\partial t} = - \sum_{n \neq m} [P_n(t)W_{n \rightarrow m} - P_m(t)W_{m \rightarrow n}], \quad (3.2)$$

where $P_n(t)$ is the probability of the system being in state n at time t and $W_{n \rightarrow m}$ is the transition rate for $n \rightarrow m$. In equilibrium $\partial P_n(t)/\partial t = 0$ then the two terms

on the right–hand side of Eq. (3.2) must be equal. This is known as the detailed balance

$$P_n(t)W_{n \rightarrow m} = P_m(t)W_{m \rightarrow n}. \quad (3.3)$$

Usually, the probability in Eq. (3.3) is not exactly known because of the partition function. To avoid this difficulty, the Markov chain of states is used. This idea, a state f th is directly created by a previous state i th, the relative probability is the ratio of the individual probabilities and does not depend on the partition function. As a result, only the energy difference between the two states is needed, e.g.

$$\Delta E = E_f - E_i, \quad (3.4)$$

when E_i and E_f are the energy of an initial state i and a final state f of the system, respectively. Any transition rate which satisfies detailed balance is acceptable. The first choice of the transition rate used in statistical physics is the Metropolis form

$$W_{i \rightarrow f} = e^{-\Delta E/k_B T} ; \Delta E > 0, \quad (3.5)$$

$$W_{i \rightarrow f} = 1 ; \Delta E < 0. \quad (3.6)$$

The Metropolis algorithm can be described by a simple recipe [29, 31].

1. Set up initial conditions, e.g., a number of lattice sites, initial states of spins and temperatures, etc.
2. Select a spin randomly. Generate a final state randomly and calculate $W_{i \rightarrow f} = e^{-\Delta E/k_B T}$.
3. Generate a random number r in the interval $(0, 1)$.
4. Flip the spin if $W_{i \rightarrow f} > r$, otherwise reject the flip.
5. Calculate and store variables A_n for each step.
6. Go to (2).
7. Finally, average variables $\langle A \rangle_n$.

Any processes can be shown as the flow chart in figure 3.1.

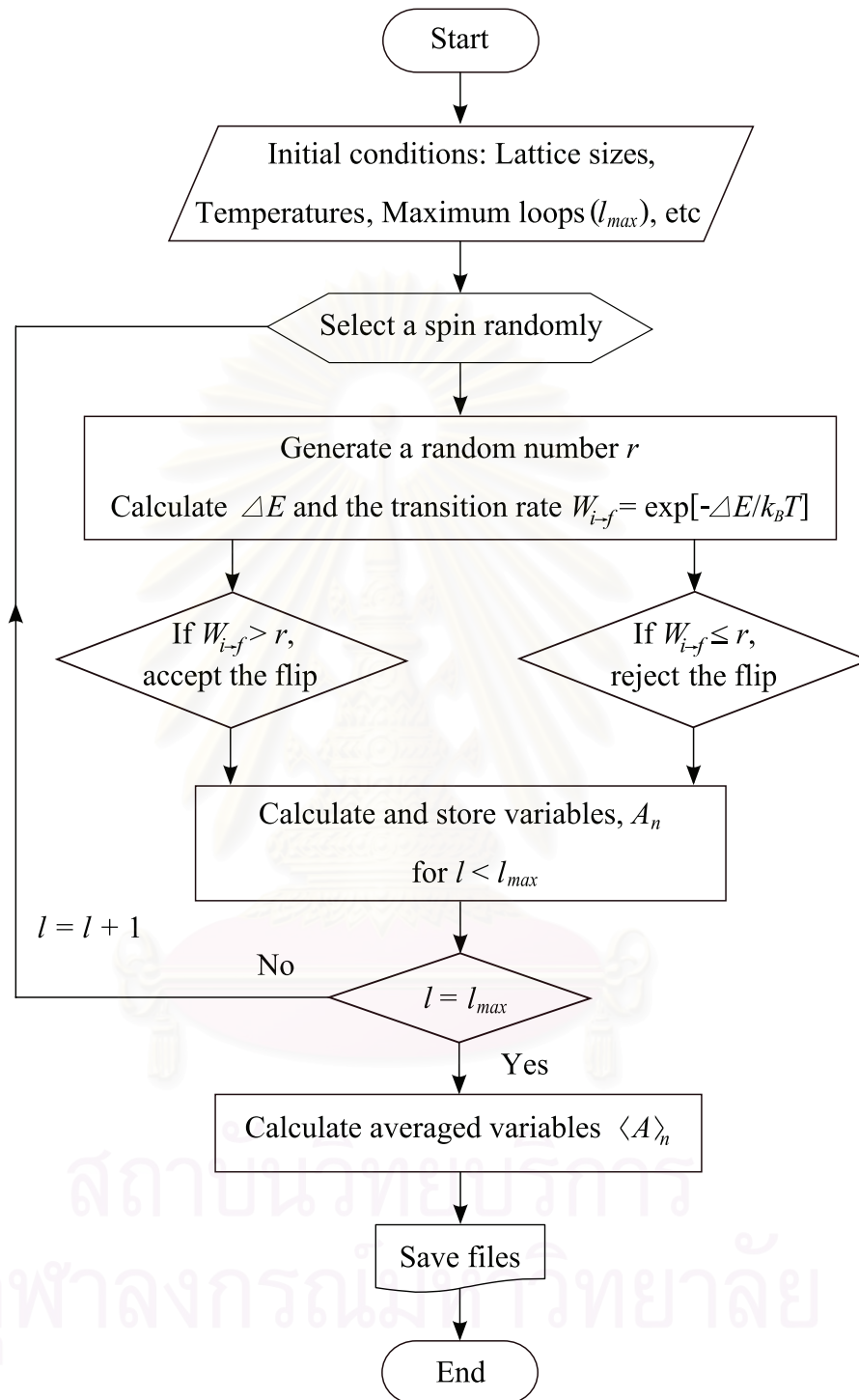


Figure 3.1: A flow chart of our simulation in the FAXY model.

CHAPTER IV

Results and Discussions

We use the Monte Carlo simulations with the frustrated antiferromagnetic XY ($FAXY$) model on the triangular lattice. In our simulations, ‘time’ is measured as the Monte Carlo step per spin (MCS). It is not necessary that any spins in a lattice must be chosen in 1 MCS because spins in a lattice are chosen randomly. The parameters which we vary in our simulations are the system sizes and the temperatures. We use linear system sizes (L), 12×12 , 24×24 , 48×48 , 72×72 , 96×96 and 120×120 . The system is set in a high temperature state (or in the ground state), after that the temperature will be decreased (or increased). At early time, the evolution of the energy of the system depends on time. However, at later time, the time independent of the energy of the system will occur at the equilibrium time (τ_{eq}), so we can say that the system will be in an equilibrium state after the equilibrium time. The equilibrium time depends on the system sizes and the temperatures. Because the correlation time becomes infinity at the critical temperatures, then the equilibrium time also becomes infinity at the same temperatures. This is true only for the infinite system size. For finite system sizes the correlation time and the equilibrium time never go to infinity. However the equilibrium time at the critical temperatures is still longest. We therefore use the equilibrium time at a temperature close to the critical temperatures to represent the equilibrium time of all temperatures for the same system size.

The equilibrium time can be obtained by plotting the energy of the system versus time as shown in figure 4.1. The energy of the system decreases with increasing time and fluctuates around some value at the equilibrium time. After

the equilibrium time, we assume that the system is already set in an equilibrium state. Also, the equilibrium time can be determined by the order parameters in the same manner. But, the equilibrium time of the order parameters is usually slightly higher than the equilibrium time of the energy of the system.

When the simulations go through each 1 MCS any important variables will be stored. However, where the system is near critical points any subsequent states separated by 1 MCS are highly correlated, then we measure any variables every 2, 5 and 10 MCSs to save unnecessary computations.

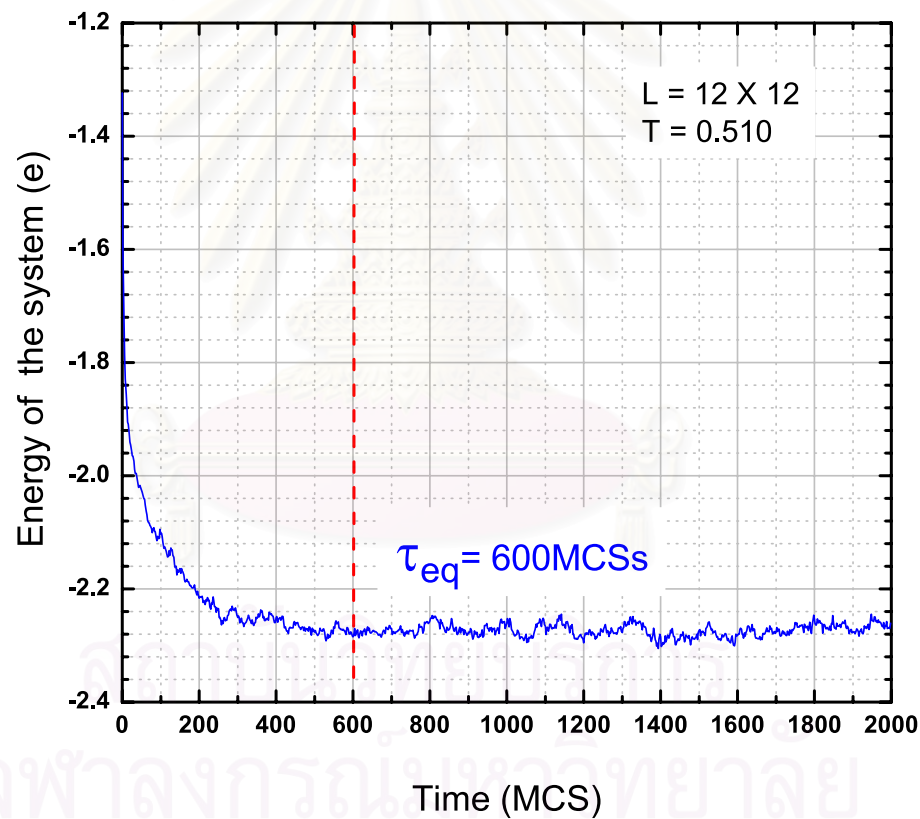


Figure 4.1: The time evolution of the energy of 12×12 lattice sites at the temperature, $T = 0.510$, the equilibrium time of the system is approximately 600 MCSs which is marked by the dash line.

4.1 The spin and the staggered chirality configurations

We observe the spin and the staggered chirality configurations of 240×240 lattice sites at equilibrium states and at different temperatures, $T = 1.0000$, 0.5130 (T_I), 0.5098 (T_{KT}), 0.2500 and 0.0001 .

Figure 4.2 shows the spin configurations in the same sublattice, where the colors represent the angles of the spins respected to an arbitrary direction. In figure 4.2(a) or at $T = 1.0000$, the spins align randomly in all directions so the net magnetization is zero at this temperature. We cannot see a group of the spins or a domain of the spins which align in the same direction, it means that the correlation length at this temperature is infinitely small. In figure 4.2(b) or at $T = 0.5130$, we can see that the domains of the spins occur with some directions; however, the net magnetization is still zero. The correlation length at this temperature is greater than zero. In figure 4.2(c) or at $T = T_{KT} = 0.5098$, the domain sizes are bigger and they increase with decreasing the temperature through the T_{KT} as a scaling form. The net magnetization increases from zero to a finite value through this temperature. In figure 4.2(d) or at $T = 0.2500$, we can see that the spins align in some directions corresponding to the broken symmetry of the system. The net magnetization is obviously non-zero and the domain sizes still increase corresponding to increasing the correlation length. In figure 4.2(e) or at $T = 0.0001$, the spins almost align in the same direction. The net magnetization and a single domain size approach their maximum values.

Similarly, the staggered chirality configurations are shown in figure 4.3, the colors represent the values of the staggered chirality. At high temperatures, $T \geq T_I$, as shown in figure 4.3(a) and 4.3(b) in which the system undergoes a short range order, the results are the same with the magnetization. At low temperatures, for Z_2 symmetry the system undergoes a long range order but for $U(1)$ symmetry the system, actually, undergoes a quasi-long range order so we can see that the

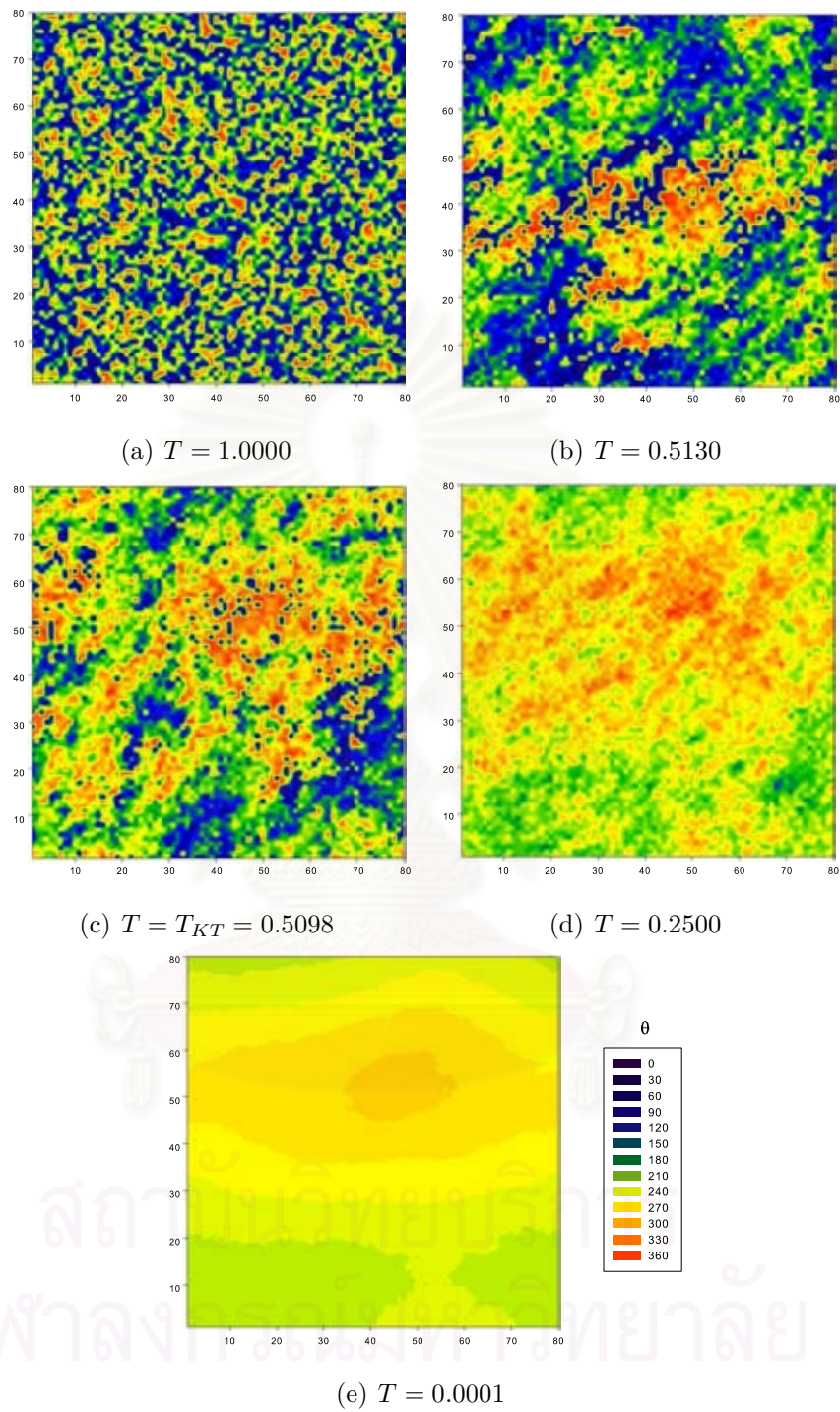


Figure 4.2: The spin configurations of $L = 240 \times 240$ at different temperatures, the colors represent the angles of the spins respected to an arbitrary direction.

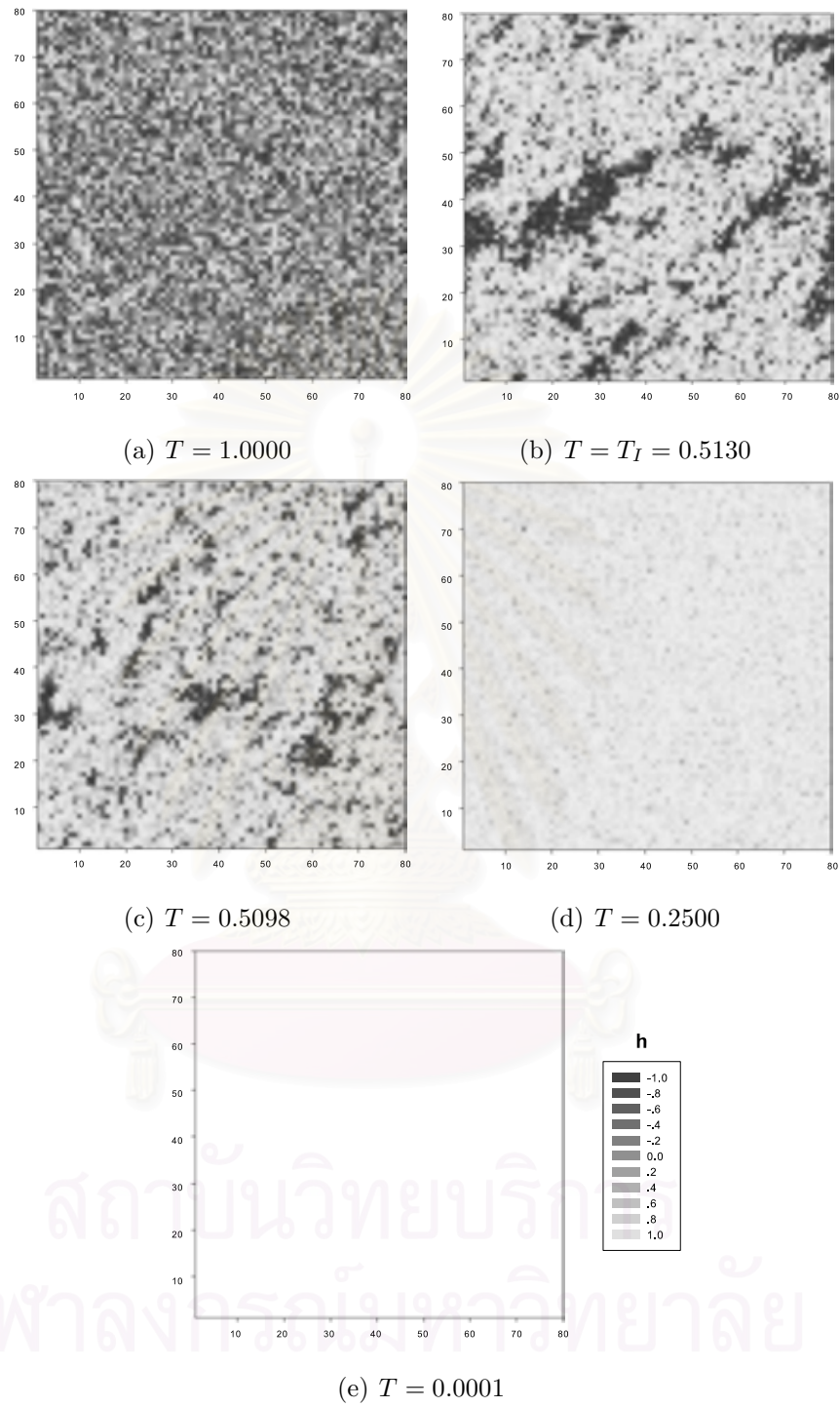


Figure 4.3: The staggered chirality configurations of $L = 240 \times 240$ at different temperatures, the colors represent the values of the staggered chirality.

domain sizes of the staggered chirality are bigger than those of the spins at the same temperature. The staggered chirality almost aligns in the same direction at $T = 0.2500$ or in figure 4.3(d) and it completely becomes the same direction at $T = 0.0001$ as shown in figure 4.3(e).

4.2 Critical temperatures

In our model, the system has the continuous $U(1)$ symmetry and the additional Z_2 symmetry that can be broken through the critical temperatures T_{KT} and T_I , respectively. To determine the critical temperatures, we use the Binder cumulants defined in Eq. (2.14) and Eq. (2.15). The Binder cumulants are stored every 5 MCSs. The simulation time is up to 500,000 MCSs and we average the Binder cumulants over 10 independent runs. The Binder cumulants will be plotted against temperature at different system sizes. The critical temperatures can be determined by the crossing points of them.

4.2.1 The Kosterlitz–Thouless transition temperature

The first critical temperature T_{KT} can be determined by B_m which is shown in figure 4.4, at small system sizes the crossing points of them depend on the system sizes. But at the larger system sizes, the crossing point is independent of the system sizes, so this point indicates the critical point of the system. The dash line placed along y axis crosses x axis at the critical temperature and then we estimate $T_{KT} = 0.509(8)$, where the last significant figure is an approximation. This temperature is slightly higher than those results [14, 22].

4.2.2 The Ising–like transition temperature

The critical temperature T_I can be determined by B_h which is shown in figure 4.5, we estimate that $T_I = 0.513(0)$. Similar to those found in the previous section, the

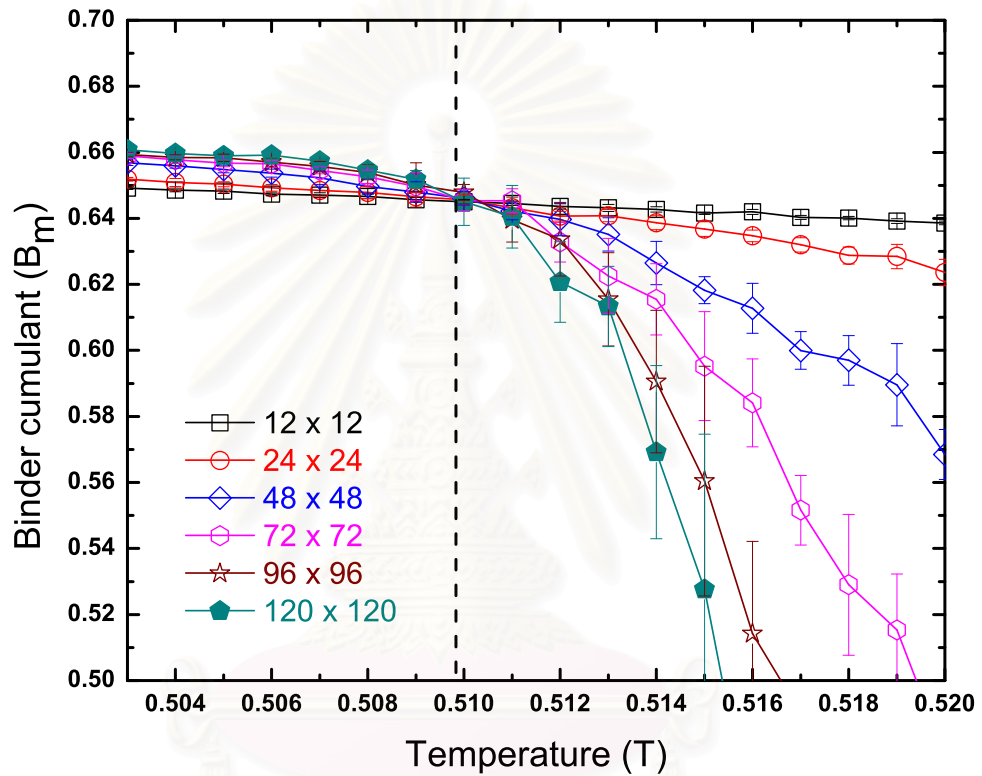


Figure 4.4: The Binder cumulant for the magnetization is plotted against the temperature at different system sizes. The dash line marks the critical temperature $T_{KT} = 0.509(8)$.

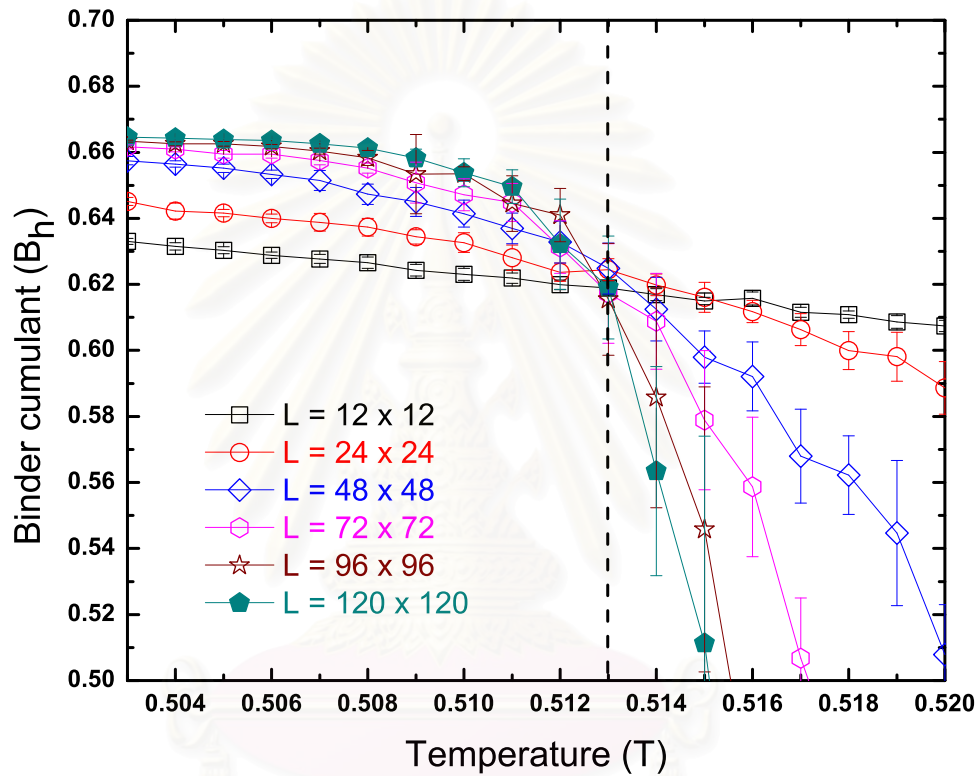


Figure 4.5: The Binder cumulant for the staggered chirality is plotted against the temperature at different system sizes. The dash line marks the critical temperature $T_I = 0.513(0)$.

crossing point is independent of the system sizes for larger system sizes. The T_I in our model is in good agreement with those results in Ref. (5, 22), and slightly higher than those results in Ref. (14).

From the results, we found that the broken symmetries clearly occur at the two separate critical temperatures, $T_{KT} < T_I$. However these temperatures lie close to each other about 0.6% compared to the lower temperature. The close temperatures were also found in these models [14, 22]. In an experiment, the exchange energy (J) is in order of $\sim 10^{-3}\text{eV}$, for example, the exchange energy of silicon in presence of a magnetic field is -0.721meV and in absence of a magnetic field is -5.232meV [36]. Then if J equals -1meV , T_{KT} and T_I are approximately 5.914K and 5.951K, respectively.

4.3 The energy of the system

In this section, the energy of the system which is written in Eq. (2.7) will be discussed. The energy of the system is stored every 10 MCSs. The simulation time is up to 1,000,000 MCSs. Then at one point of any temperatures the energy of the system is averaged over 100,000 independent microstates. In figure 4.6, the energy is plotted against the temperature at different system sizes. At high temperatures, the energy of the system decreases with decreasing the temperature. At the critical temperatures, the energy of the system decreases faster than other temperatures due to the broken symmetries of the system. At low temperatures, the energy of the system approaches -3 in limit $T \rightarrow 0$. Then the energy of the system becomes the minimum energy which equals to $-3|J|$ corresponding to the 120° structure in the ground state.

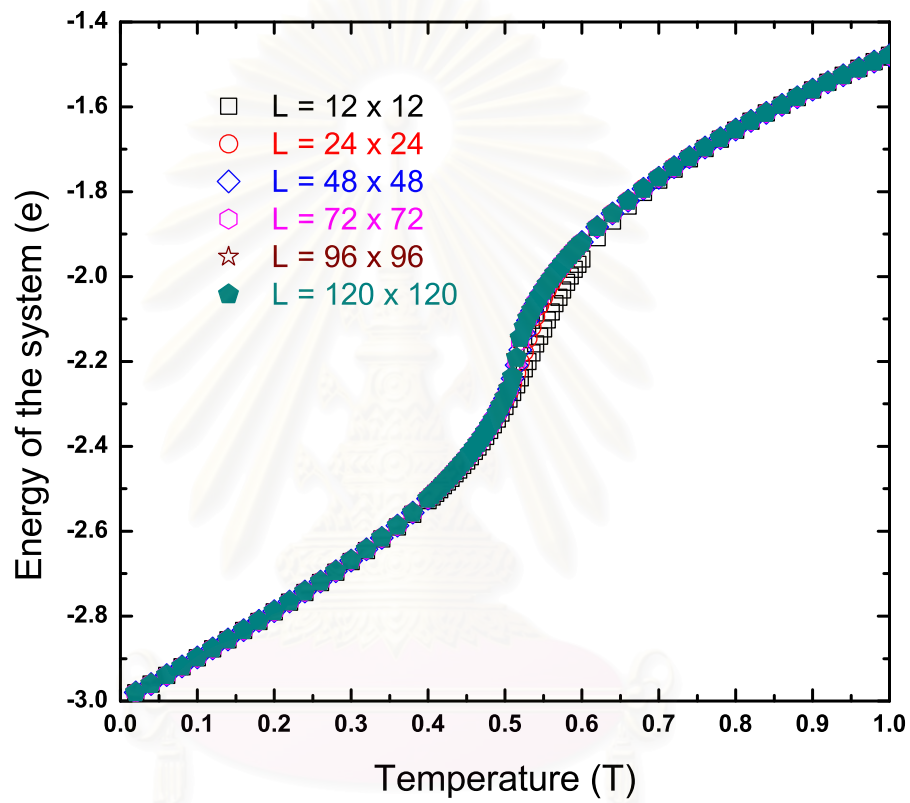


Figure 4.6: The energy of the system is plotted against the temperature at different system sizes.

4.4 Order parameters

From previous chapter we introduce the order parameters which imply the spontaneous symmetry breaking. The order parameters in our model, the sublattice magnetization and the staggered chirality will be discussed in this section. The order parameters are stored every 10 MCSs. The simulation time is up to 1,000,000 MCSs. After that, the order parameters will be averaged.

4.4.1 The sublattice magnetization

In figure 4.7, the sublattice magnetization, the order parameter for the $U(1)$ symmetry breaking transition, is plotted against the temperature at different system sizes. The system size dependence of the sublattice magnetization is divided into two regions. At high temperatures, there is a strong finite size effect so the net magnetization is non-zero. However, this effect decreases with increasing the system size then the magnetization becomes zero as $L \rightarrow \infty$. Also, the sublattice magnetization approaches zero when the temperature goes to infinity. In this region, spins lie in all directions randomly then the system is said to be a disordered state. At low temperatures, the system size dependence of the sublattice magnetization is caused by the thermal fluctuation. When the temperature decreases to zero the sublattice magnetization approaches 1, then the system is said to be an ordered state.

Actually, for $T \leq T_{KT}$, the thermal fluctuation induces the system to be a quasi-long range order state, the sublattice magnetization has asymptotic behavior as $m_A \sim L^{-x}$ when x is an exponent and depends on temperatures. In figure 4.8, the sublattice magnetization is plotted against the system size at different temperatures. Clearly the sublattice magnetization follows the asymptotic form at $T \leq T_{KT}$. The exponent x is determined by a slope of log-log scale plot which is marked by the dash line. The theory predicts that the exponent $x = 1/8$ at the critical temperature [24, 25, 34]. In our simulation, we estimate that $x \simeq 0.16$ at

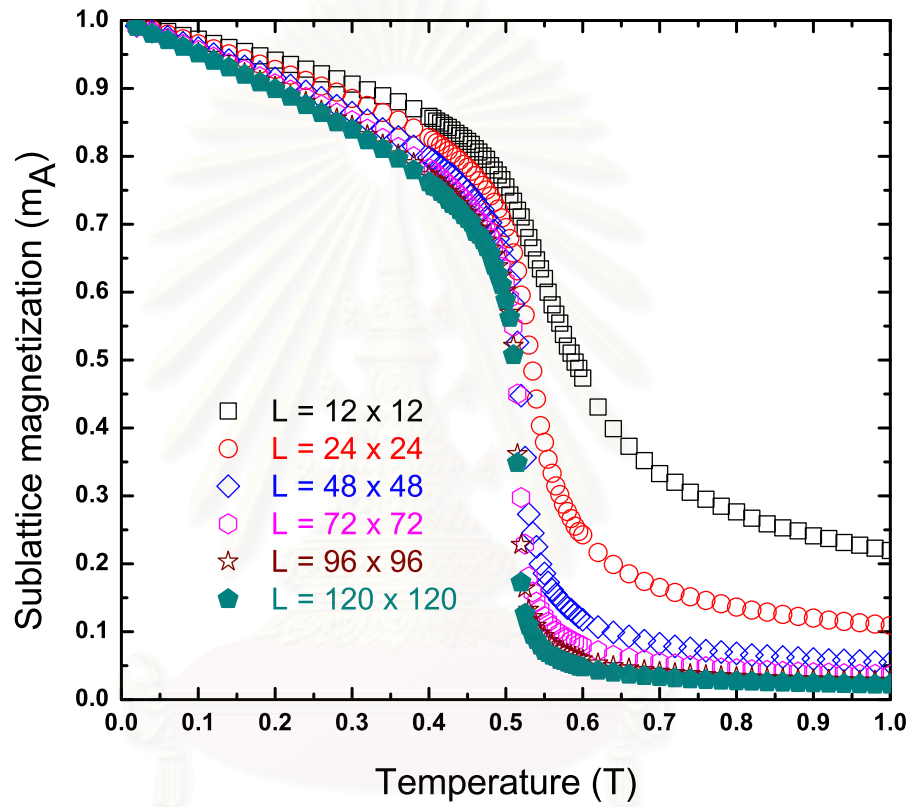


Figure 4.7: The sublattice magnetization is plotted against the temperature at different system sizes.

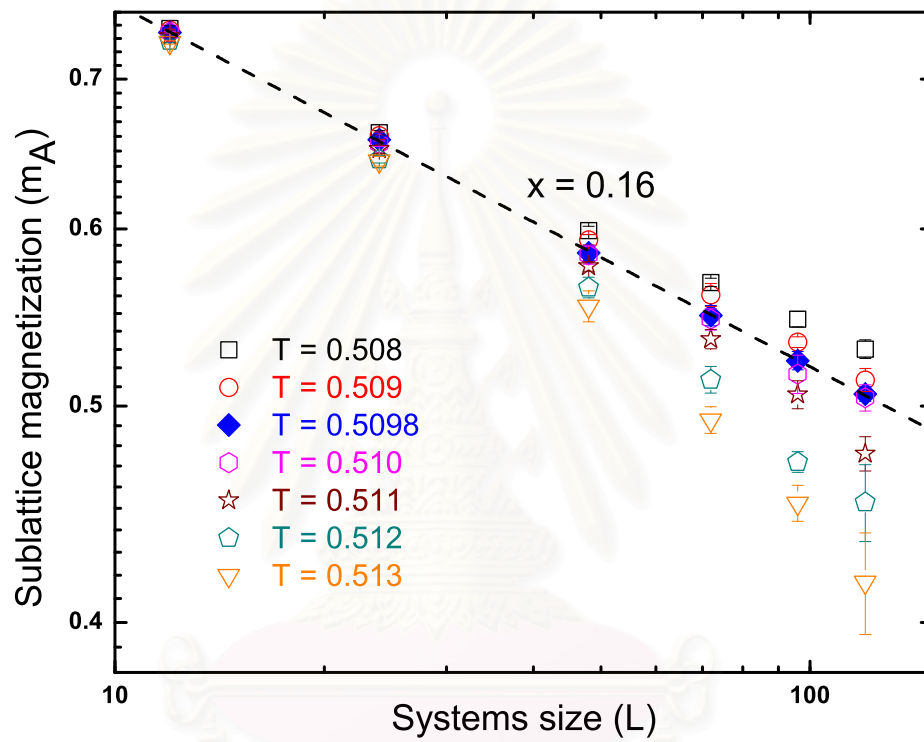


Figure 4.8: The sublattice magnetization near the critical temperature $T \leq T_{KT}$ is plotted against the system size at different temperatures. The dash line has a slope -0.16 at $T = T_{KT}$.

$T = T_{KT}$ which is slightly higher than that value but in good agreement with a result reported in Ref. (18).

4.4.2 The staggered chirality

Next result is the staggered chirality which is the order parameter for the Z_2 symmetry breaking transition. In figure 4.9, the staggered chirality is plotted against the temperature at different system sizes. At high temperatures, the finite size effect still holds the value of the order parameter and this effect decreases with increasing the system size. However, this effect is less than that of the sublattice magnetization for small system sizes. But for larger system sizes, the influence of the effect is small both the sublattice magnetization and the staggered chirality. We can see that the staggered chirality goes to zero as $L \rightarrow \infty$. It indicates that the system is in a disordered state. At the critical temperature, the staggered chirality increases continuously from zero to a finite value. At low temperatures, the finite size effect is small so the staggered chirality of different system sizes is merged into a single line. If the system size is larger, the staggered chirality will not depend on the system size. Moreover, the finite staggered chirality increases with decreasing the temperature and approaches 1 when the temperature goes to zero. It indicates that the system is in an ordered state below the critical temperature and in the ground state at $T \approx 0$. As the results, the ground state of the system can be found by considering the order parameters as well as the energy of the system.

One more interesting point, the critical behavior of the staggered chirality near the critical temperature follows Eq. (2.33) as $h \sim (-t)^\beta$. This equation is true only below the critical temperature or as $t \rightarrow 0^-$. In figure 4.10, the staggered chirality is plotted against the reduced temperature at different system sizes. For small system sizes, the power law of the staggered chirality does not occur evidently due to the finite size effect. But, for larger system sizes, the staggered chirality becomes the asymptotic behavior as $t \rightarrow 0^-$. In the figure, the

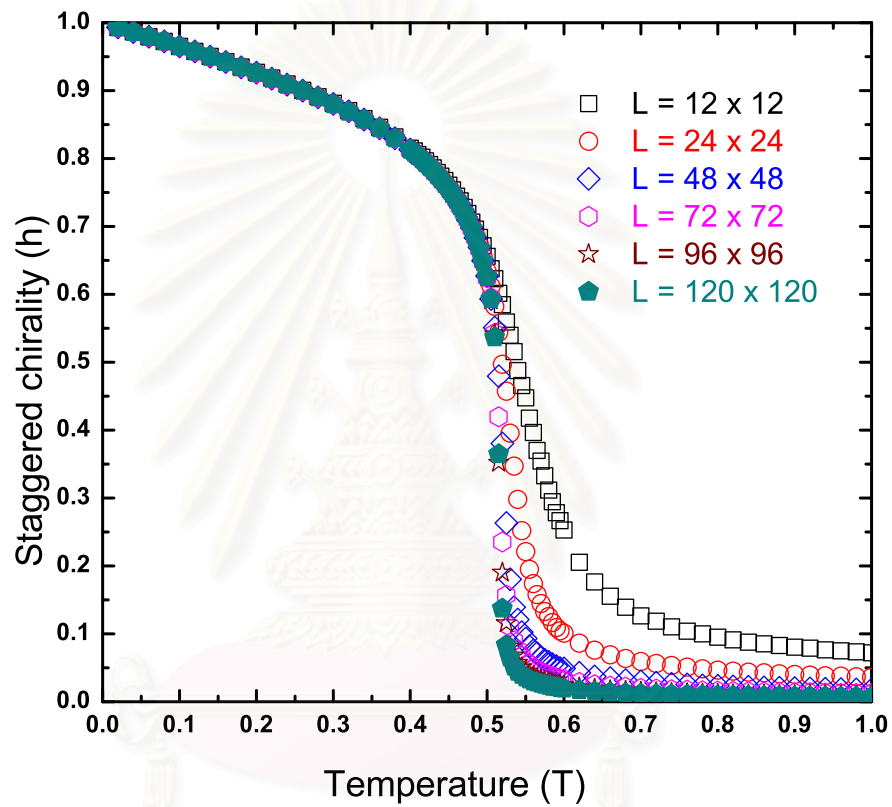


Figure 4.9: The staggered chirality is plotted against the temperature at different system sizes.

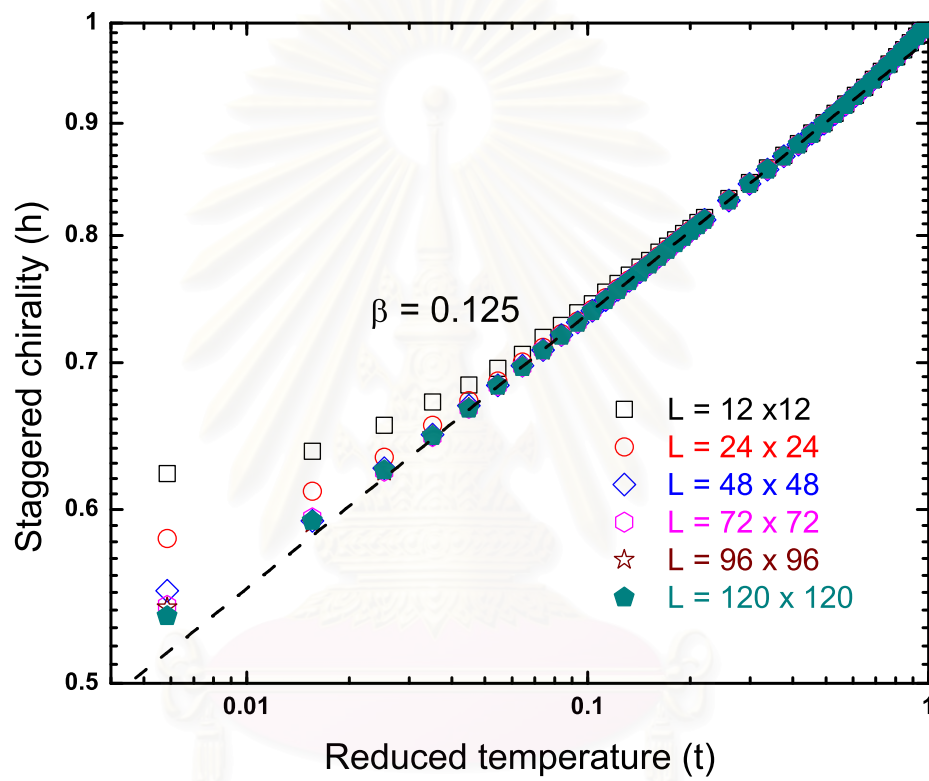


Figure 4.10: The staggered chirality is plotted against the reduced temperature at different system sizes. The dash line has a slope = 0.125.

dash line indicates the critical exponent β and we estimate that $\beta = 0.125$. Our value is in good agreement with the exact value, $\beta = 1/8$. This value is known as the Onsager solution of the two-dimensional Ising model on the square lattice.

4.5 The specific heat

In critical phenomena, the fluctuations have been one of interesting properties of the system. These can indicate the critical state of the system. The first parameter, the specific heat, related to the fluctuation relation of the energy will be discussed in this section. The specific heat can be written as Eq. (2.12). For the second order phase transition, the specific heat has a finite value both above and below critical temperatures, but diverges at critical temperatures corresponding to the slope of the energy of the system at critical temperatures. In the figure 4.11, the specific heat is plotted against the temperature at different system sizes. Each point, the specific heat is stored every 10MCSs and the simulation time is up to 1,000,000 MCSs. We can see that, at high temperatures, the specific heat decreases with increasing the temperature and approaches to zero when the temperature goes to infinity.

Also, near the critical temperatures, the specific heat depends on the system size due to the finite size effect. Moreover, the peak's value of each system size increases and the position of the peak moves toward the critical temperatures as $L \rightarrow \infty$. It seems that the specific heat will diverge if the size of the system goes to infinity. It indicates that the system changes from a disordered phase to an ordered phase through the second order phase transition.

At low temperatures, the specific heat decreases with decreasing the temperature and approaches to a finite value when the temperature goes to zero. We can see that at this temperature range the finite size effect influences to the specific heat less than that at high temperatures.

According to the theoretical prediction in the two-dimensional Ising model,

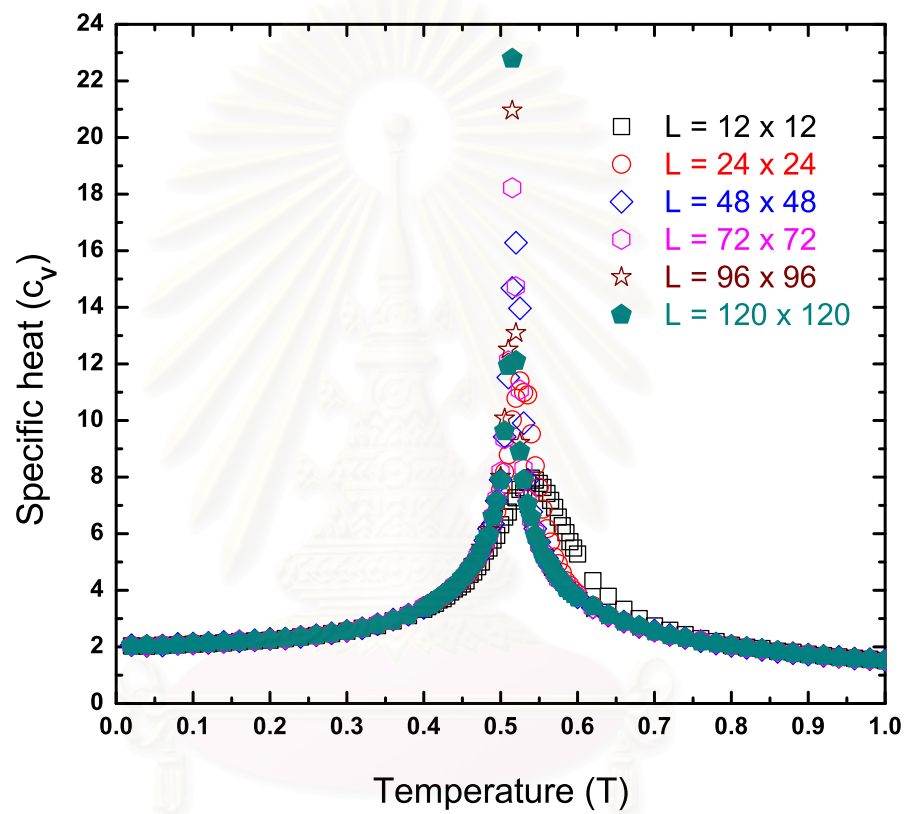


Figure 4.11: The specific heat is plotted against the temperature at different system sizes.

the Onsager solution [30], the specific heat diverges logarithmically near the critical temperatures as $c_V \sim \log|t|$, so the critical exponent α in Eq. (2.32) must be zero. Another suggestion, for a finite system size, the peak of the specific heat depends on the system size as $c_{V_*} \sim L^{\alpha/\nu}$ [31] near the critical temperatures. Here, c_{V_*} is the peak of the specific heat, so the specific heat diverges as $L \rightarrow \infty$. Similarly, for the Ising universality class, the critical exponent α equals zero and then the specific heat shows a logarithmic divergence as $c_{V_*} \sim \log(L)$.

Now, we want to know that the specific heat follows the logarithmic divergence or the power law then we plot the specific heat versus the reduced temperature as shown in figure 4.12 and figure 4.13. In figure 4.12, the specific heat is plotted against the reduced temperature in the log–log scale. The specific heat splits into two curves for the system located at high temperature states as shown in figure 4.12(a) and at low temperature states as shown in figure 4.12(b). The upward curve corresponding to the system being in low temperature states and the downward curve corresponding to the system being in high temperature states. But when the temperature of the system decreases (increases) to the critical temperatures, the specific heat merges into a single line as shown in figure 4.12(c). This line shows the power law of the specific heat and it indicates the critical exponent α , then we estimate that $\alpha = 0.45$. For $t \rightarrow 0^+$ and $t \rightarrow 0^-$, it is hard to obtain the asymptotic behavior of the specific heat due to the strong finite size effect is near the critical temperatures. Next we look at figure 4.13, the specific heat is plotted against the reduced temperature in the semi–log scale. Clearly, the specific heat does not follow the logarithmic behavior both in high temperature states and in low temperature states as shown in figure 4.13(a), 4.13(b) and 4.13(c). This result supports the power law of the specific heat.

Another form of the specific heat can be written as a function of the system size. In order to know how the specific heat depends on the system size, we plot c_{V_*} of the specific heat against the system size. In figure 4.14(a), c_{V_*} is plotted in the log–log scale to observe the power law behavior of the specific heat. For small system sizes, $L \leq 48$, c_{V_*} depends on the system size as a power law indicated by

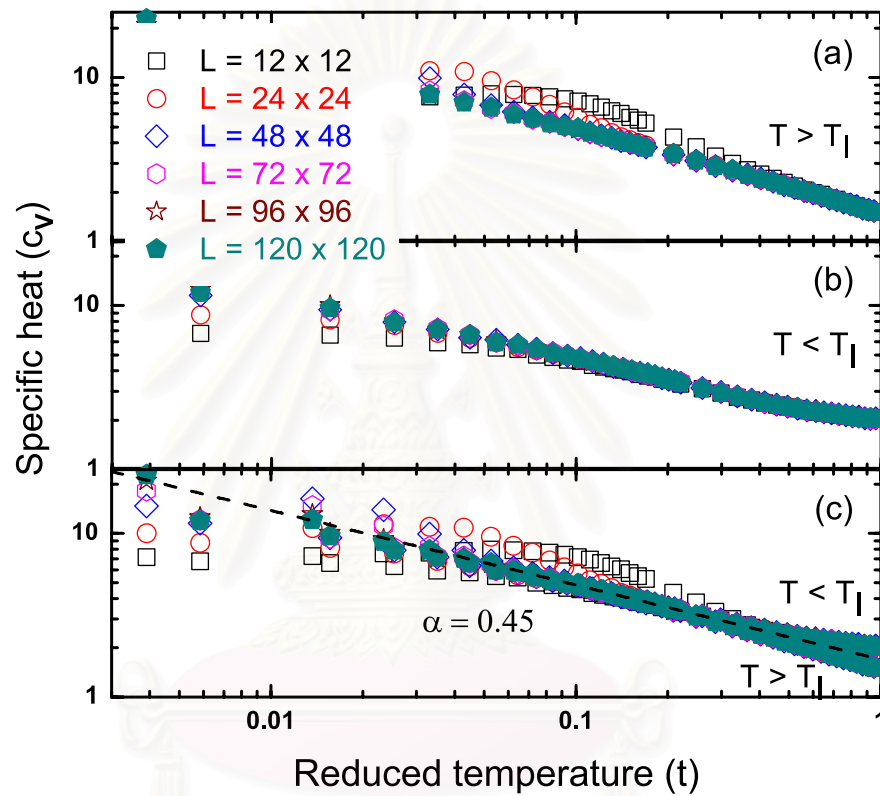


Figure 4.12: The specific heat is plotted against the reduced temperature at different system sizes. The dash line has a slope = -0.45 .

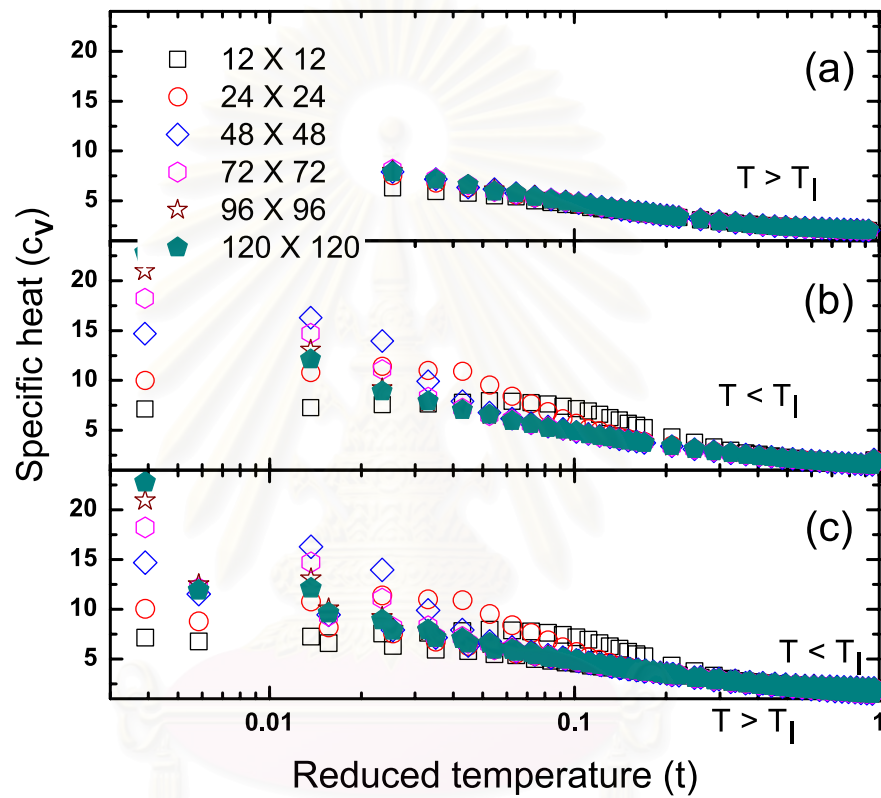


Figure 4.13: The specific heat is plotted against the reduced temperature at different system sizes.

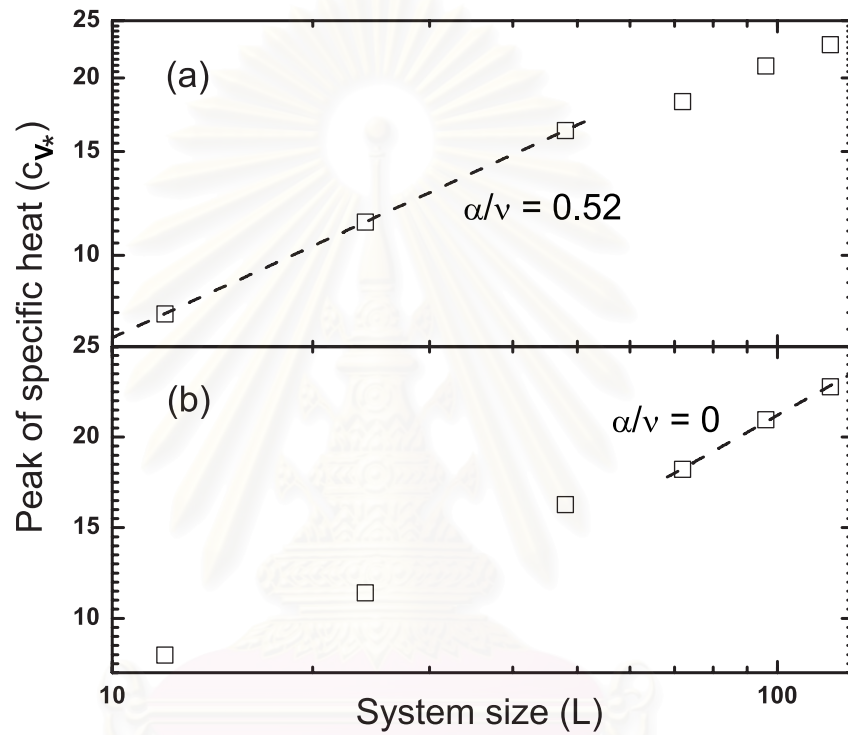


Figure 4.14: The peak of the specific heat at different system sizes is plotted against the system size, (a) the dash line indicates $\alpha/\nu = 0.52$ and (b) the dash line indicates $\alpha/\nu = 0$.

the dash line. We estimate the slope = 0.52 which is equivalent to α/ν . The result shows clearly that for small system sizes, c_{V_*} follows the power law as $c_{V_*} \sim L^{\alpha/\nu}$ rather than the logarithmic behavior which yields $\alpha = 0$. The non–logarithmic behavior was also found in Ref. (5, 6, 22, 27). For larger system sizes, $L > 48$, we can not observe any power law of c_{V_*} , we think that the peak of the specific heat is very sharp so it is highly sensitive to the temperature. As the reason, if we estimate c_{V_*} using a wide range of the temperatures, we can not obtain the value accuracy and it seems to be independent of the temperature which is shown in figure 4.11. Moreover, a calculation of a precise value of c_{V_*} will be prevented by the strong finite size effect and the highly fluctuation around the critical temperatures.

In figure 4.14(b), c_{V_*} is plotted against the system size in the semi–log scale. We can see that for the small systems, $L \leq 48$, c_{V_*} does not follow the logarithmic behavior but for the higher system sizes, it seems c_{V_*} tends toward the logarithmic behavior. This behavior was also found in Ref. (18) which illustrates that the behavior of the specific heat changes from non–logarithmic behavior to logarithmic behavior at a certain critical system size. This behavior automatically yields $\alpha = 0$. However, we can not identify that the specific heat has only the non–logarithmic behavior or it changes from the non–logarithmic to the logarithmic behavior at a critical system size due to the crude estimation of the specific heat near the critical temperatures for $L > 48$.

4.6 The magnetic susceptibility

Another interesting point is the magnetic susceptibility, which is related to the fluctuation relation of the sublattice magnetization. The magnetic susceptibility is stored every 10 MCSs. The simulation time is up to 1,000,000 MCSs. After that, the susceptibility will be averaged. In figure 4.15, the susceptibility is plotted against the temperature at different system sizes. At high temperatures, the susceptibility decreases with increasing the temperature and approaches to zero as $T \rightarrow \infty$. In this region, the susceptibility is independent of the system size. Near the critical temperatures, the susceptibility increases rapidly when the temperature goes to critical temperatures. At low temperatures, its value evidently depends on the system size. This is unlike in the case of high temperatures because the sublattice magnetization depends on the system size below the critical temperature. This behavior corresponds to the non-finite susceptibility below the critical temperatures for the infinite system size and it indicates that this transition belongs to the KT transition. However, the susceptibility has a finite value at $T = 0$.

Next, in figure 4.16, the susceptibility at high temperature states is plotted against the reduced temperature at different system sizes. The dash line and the solid line show the power law of the susceptibility near the critical temperatures and at the higher temperatures, respectively. At $t \leq 0.2$, we estimate that the critical exponent $\gamma = 1.05$ marked by the dash line. This value is slightly higher than that value in Ref. (9) but lower than those values in Ref. (6, 13) for the $FFXY$ model. At higher temperatures, $t > 0.2$, we estimate that $\gamma = 1.23$ marked by the solid line.

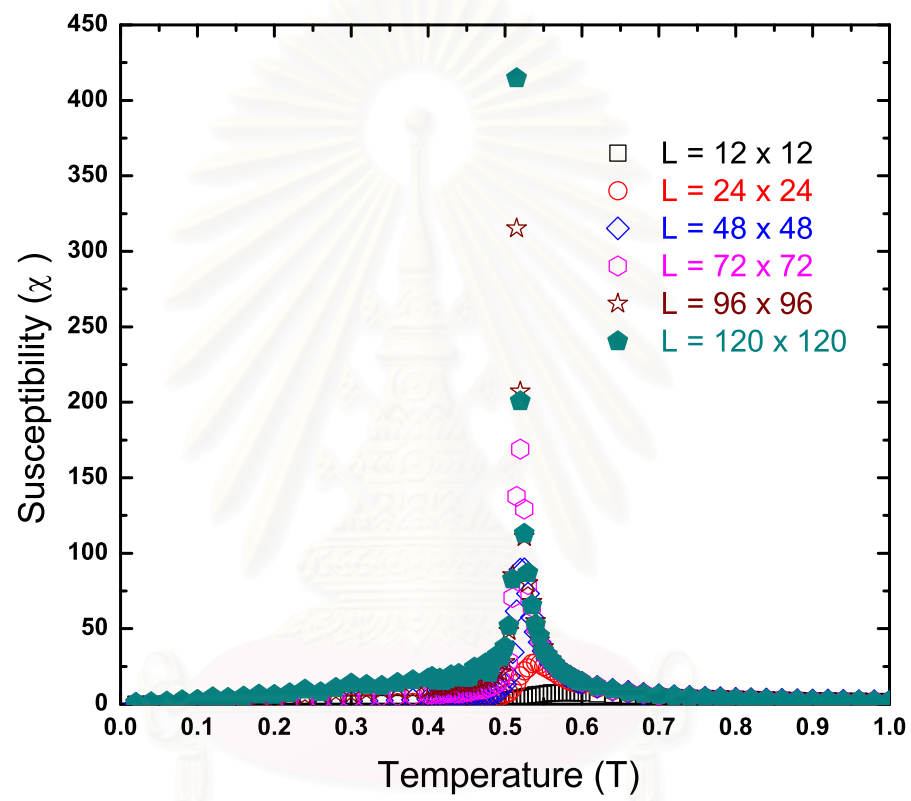


Figure 4.15: The magnetic susceptibility is plotted against the temperature at different system sizes.

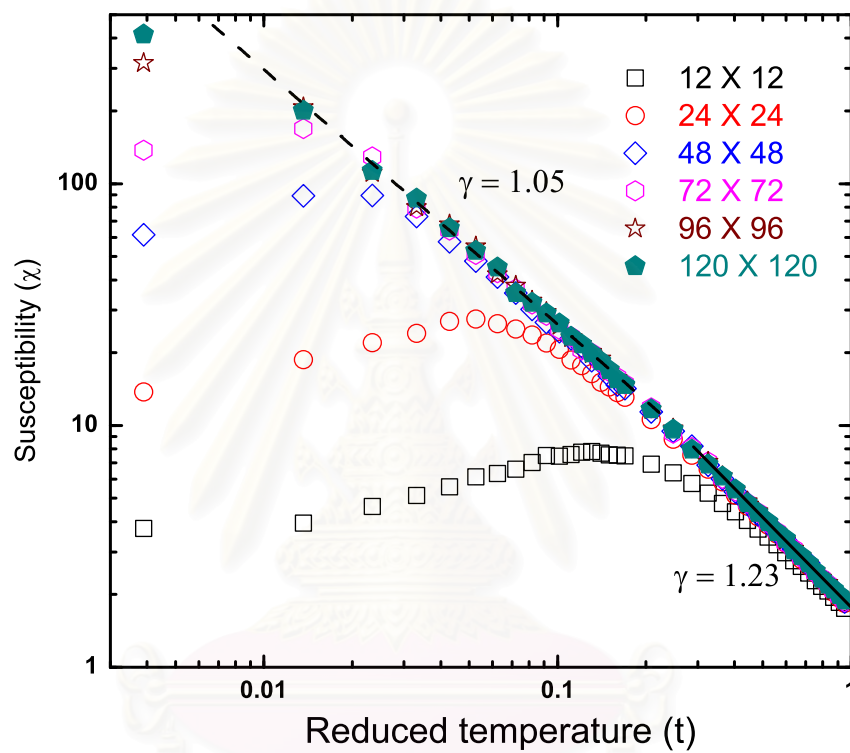


Figure 4.16: The magnetic susceptibility is plotted against the reduced temperature at different system sizes, the dash line has a slope -1.05 and the solid line has a slope -1.23 .

4.7 Correlation functions

In order to obtain the details of the behavior of the system, the correlation between spins and the correlation between chirality will be described. We use the correlation function C_m defined in Eq. (2.16) to determine the correlation between the spins and C_h defined in Eq. (2.17) to determine the correlation between the chirality. In our simulations, both correlation functions are stored every 5 MCSs and the simulation time is up to 1,000,000 MCSs. After that the correlation functions will be averaged. From the Eq. (2.21) and Eq. (2.28), the correlations decay exponentially with the distance at high temperatures and become a power law at critical temperatures. To determine the critical exponent η , the system is set in critical states so we expect that the correlation functions will decay as a power law.

4.7.1 The spin–spin correlation function

First, the spin–spin correlation function C_m is plotted against distance r at the critical temperature T_{KT} . Note that the maximum distance of each system size does not equal to the system size because we use the periodic boundary conditions and we use spins in the same sublattice to find the correlation function in the vertical direction. Then the maximum distance $r_{max} = 30$ corresponding to $L = 120$ while the minimum of r_{max} is 6 corresponding to $L = 24$. In figure 4.17, for a short distance, the correlation between the spins is quite high and decreases with increasing the distance and goes to zero as $r_{max} \rightarrow \infty$. Also the correlation of the spins decreases with increasing the system size at the same temperature.

At the critical temperature, we assume that the correlation function decays as a power law so we plot the correlation function against the distance in the log–log scale as shown in figure 4.18. For small sizes, the power law does not occur evidently but the correlation function tends to this behavior when the system size is larger. The dash line shows the power law of the correlation function at

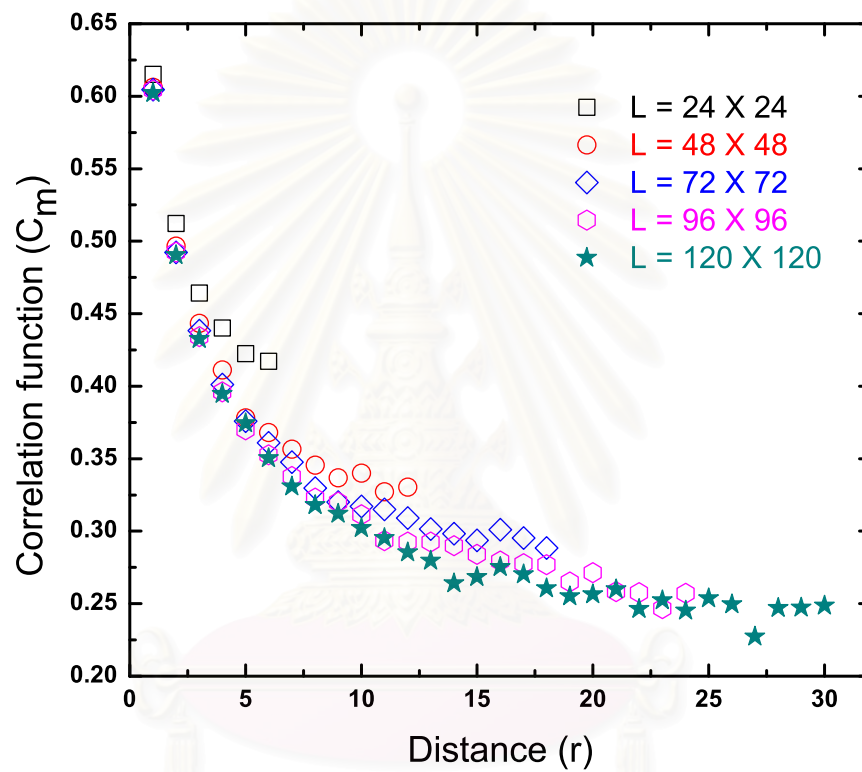


Figure 4.17: The correlation function C_m is plotted against the distance at the critical temperature T_{KT} .

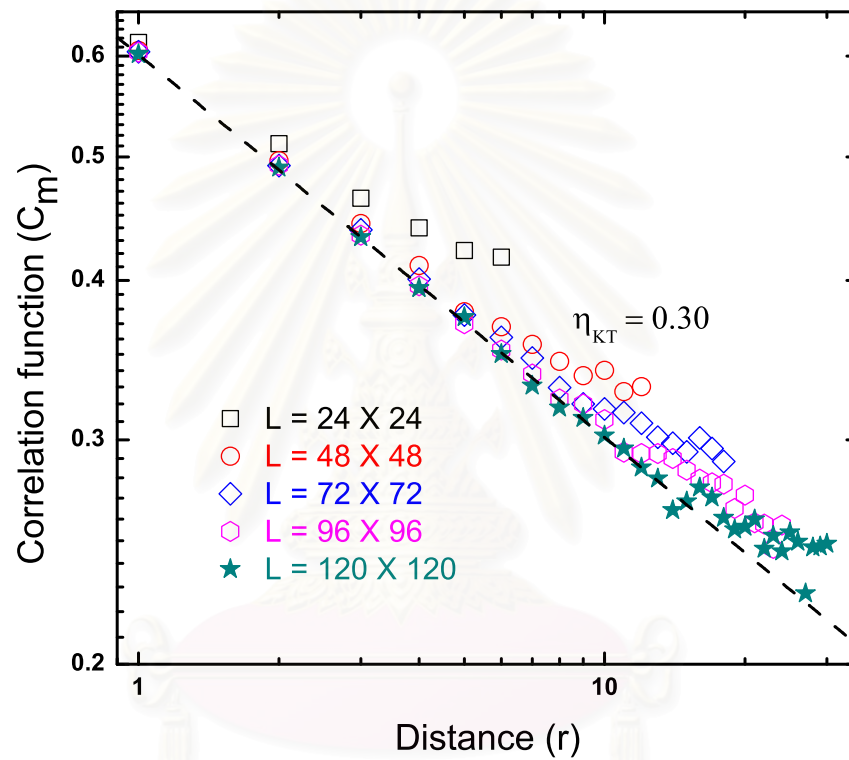


Figure 4.18: The correlation function C_m is plotted against the distance at the critical temperature T_{KT} . The dash line has a slope = -0.30 .

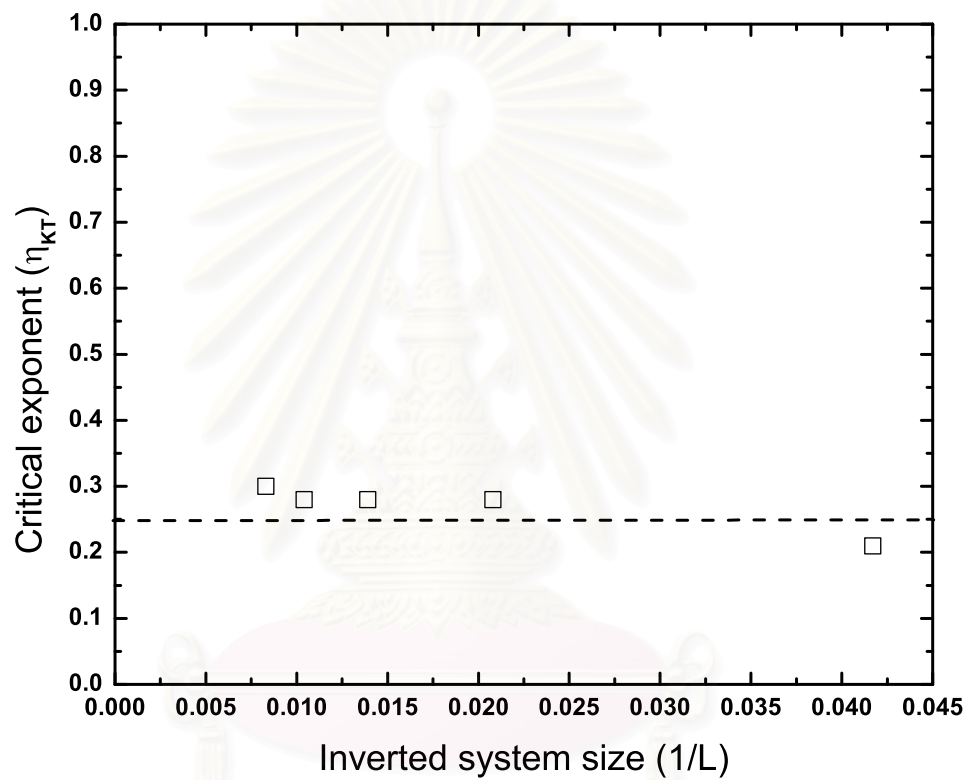


Figure 4.19: The system size dependence of η_{KT} is plotted against the inverted system size $1/L$. The dash line marks the actual value of $\eta_{KT} = 0.25$.

$L = 120$, and we estimate that the critical exponent $\eta_{KT} = 0.30$. This value is higher than the actual value $\eta_{KT} = 0.25$ [25] of the KT transition. However the difference of this value was also found in those Ref. (5, 7) for both $FAXY$ and $FFXY$ models. Moreover, actually, η_{KT} depends on the temperature below the critical temperature. It varies widely if one goes from the critical state to lower temperature states, which is shown in Ref. (19). As the reason, it may be possible that η_{KT} that we estimate is affected by the temperature.

Another interesting point, η_{KT} of different system sizes is plotted against the inverted system size ($1/L$) to show how η_{KT} depends on and what is the η_{KT} in limit $L \rightarrow \infty$ or $1/L \rightarrow 0$. In figure 4.19, the dash line marks the actual value $\eta_{KT} = 0.25$ of the KT transition at T_{KT} . The result shows that $\eta_{KT}(L = 24)$ is slightly less than that value, but for $L > 24$, η_{KT} is slightly higher than the actual value. For the system sizes, $L > 24$, η_{KT} increases slightly with L , it means that the finite size effect is not too strong, so $\eta_{KT}(L \rightarrow \infty)$ may not differ from $\eta_{KT}(L = 120)$.

4.7.2 The chirality–chirality correlation function

Next the correlation between the chirality will be discussed. In figure 4.20, the chirality correlation function C_h is plotted against the distance at the critical temperature T_I . Similarly, C_h decreases with increasing the distance and also decreases when the system size increases at the same temperature. We can see that for the same system size, C_h is less than C_m it means the correlation between the chirality is weaker than the correlation between the spins. At the same distance, C_h decreases faster than C_m when the system size increases due to the finite size effect has influence to C_h more than C_m .

From Eq. (2.28), C_h also has the logarithmic behavior at the critical temperature T_I . So in figure 4.21, C_h is plotted against the distance in the log–log scale. The dash line marks the power law of C_h at the system size $L = 120$. The approximation yields $\eta_I = 0.19$ which is lower than that of the Ising value

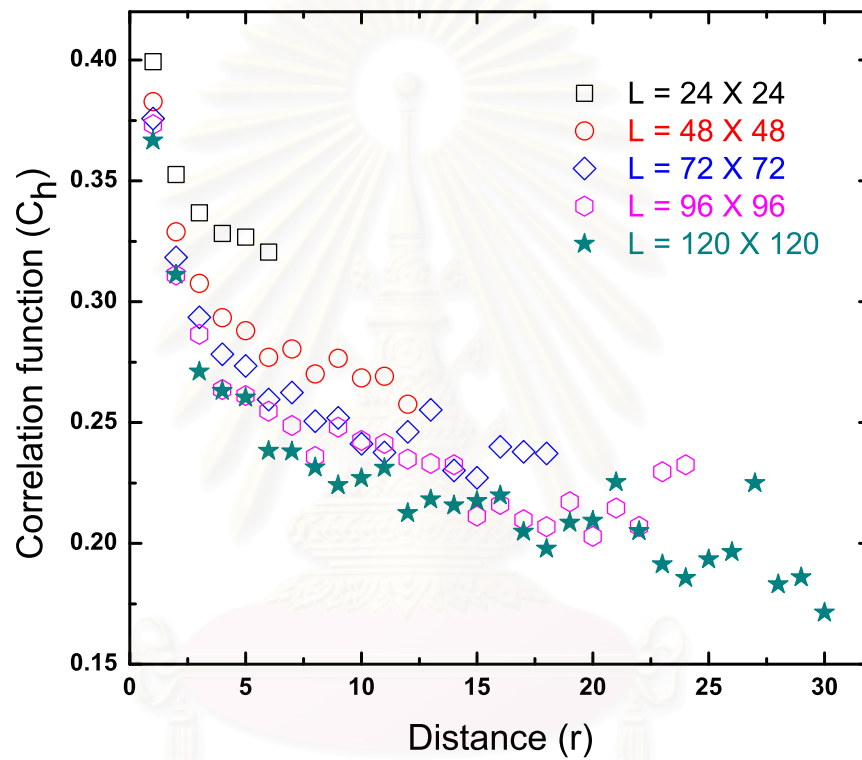


Figure 4.20: The correlation function C_h is plotted against the distance at the critical temperature T_I .

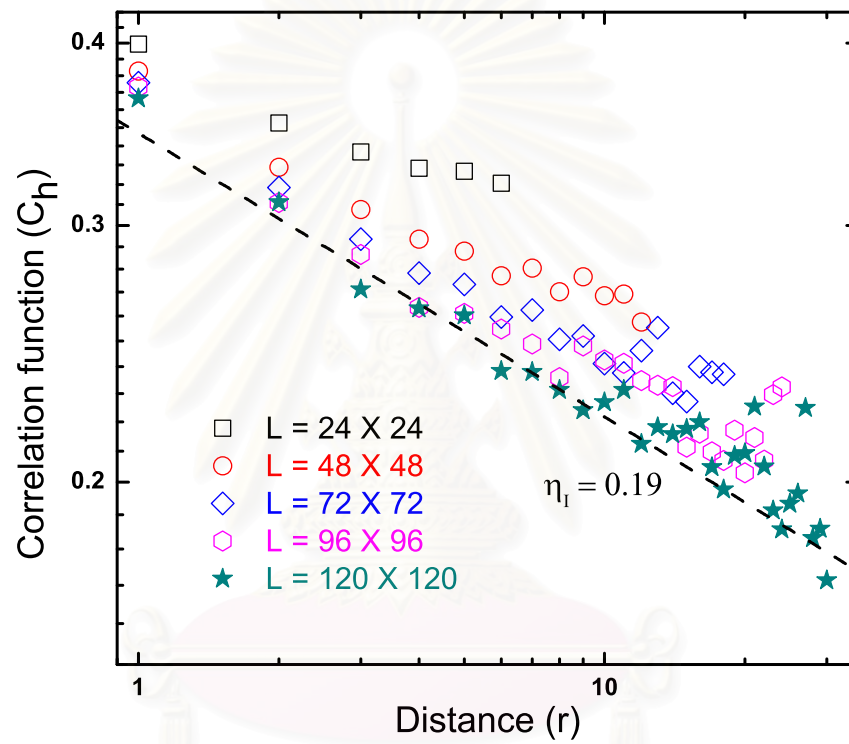


Figure 4.21: The correlation function C_h is plotted against the distance at the critical temperature T_I . The dash line has a slope = -0.19 .

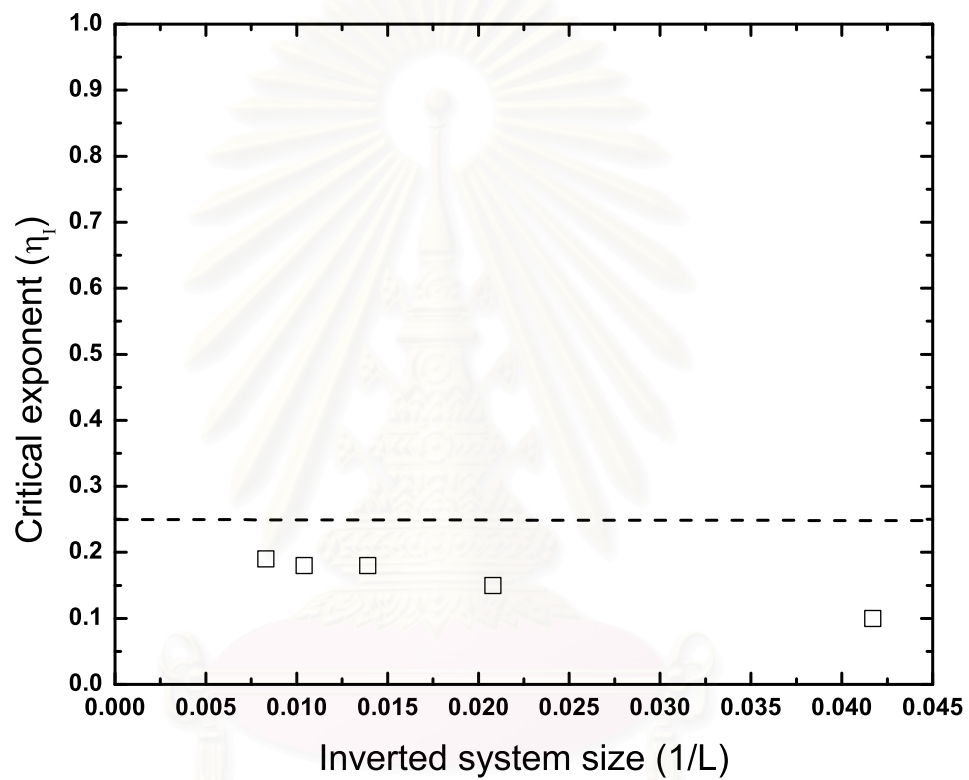


Figure 4.22: The system size dependence of η_I is plotted against the inverted system size $1/L$. The dash line marks the actual value of $\eta_I = 0.25$.

$\eta_I = 0.25$.

In figure 4.22, η_I at different system sizes is plotted against $1/L$. The dash line marks $\eta_I = 0.25$. We can see that η_I increases with increasing L . In limit $1/L \rightarrow 0$, η_I tends to that value. However, because of the strong finite size effect, η_I increases slowly with L .

4.8 Correlation lengths

To determine the behavior of the system in more details, the correlation lengths ξ will be considered. In simulations, ξ are stored every 2 MCSs and the simulation time is up to 400,000 MCSs. After that the correlation lengths will be averaged. The correlation lengths are only observed in high temperature states.

4.8.1 The correlation length of spins

In figure 4.23, the correlation length of spins ξ_m is plotted against the reduced temperature at different system sizes. We can see that ξ_m increases with decreasing the reduced temperature and it has a maximum value at T_{KT} or at $t = 0$. At the temperature ξ_m increases with increasing the system size and it diverges when the system size goes to infinity. For small system sizes, $L \lesssim 24$, the correlation length increases slowly with decreasing the reduced temperature, while at the larger system sizes, the correlation length increases more faster than that of those sizes. The increasing of the correlation length occurs evidently near the critical temperature or at $t \rightarrow 0$.

In order to know the behavior of the correlation length, we plot ξ_m against the reduced temperature in the log–log scale. Since ξ_m from Eq. (2.22) diverges faster than a power law so we expect that for larger system sizes the upward curve of ξ_m will occur. In figure 4.24, for $L \leq 72$ a signal of the upward curve does not occur at all temperatures. But, for $L > 72$ we can observe the behavior

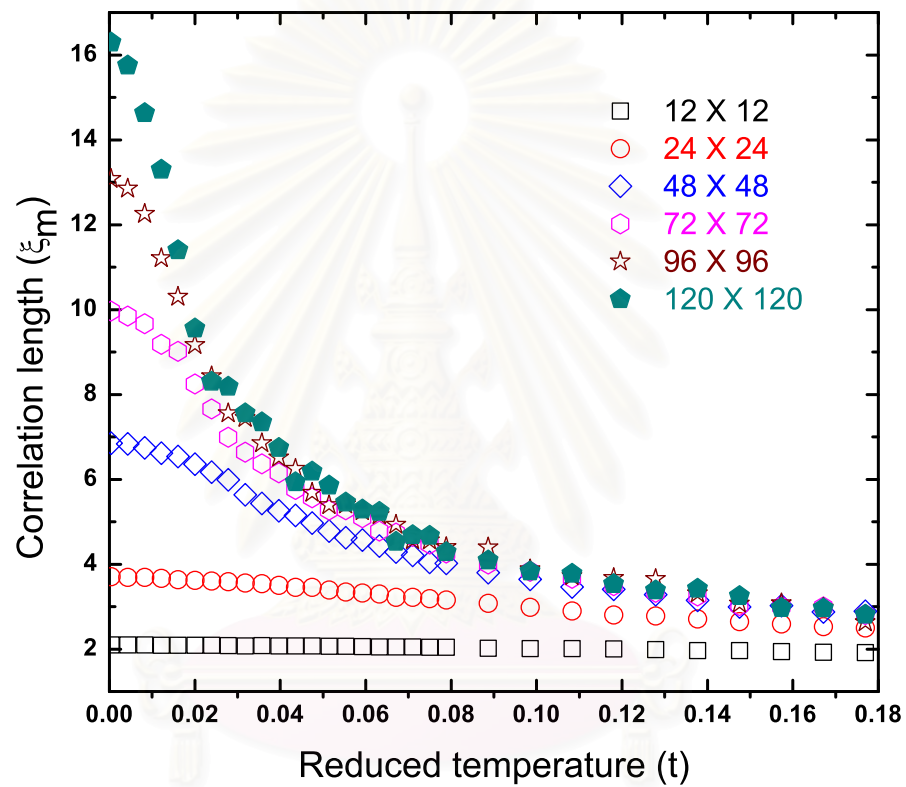


Figure 4.23: The correlation length ξ_m is plotted against the reduced temperature at different system sizes.

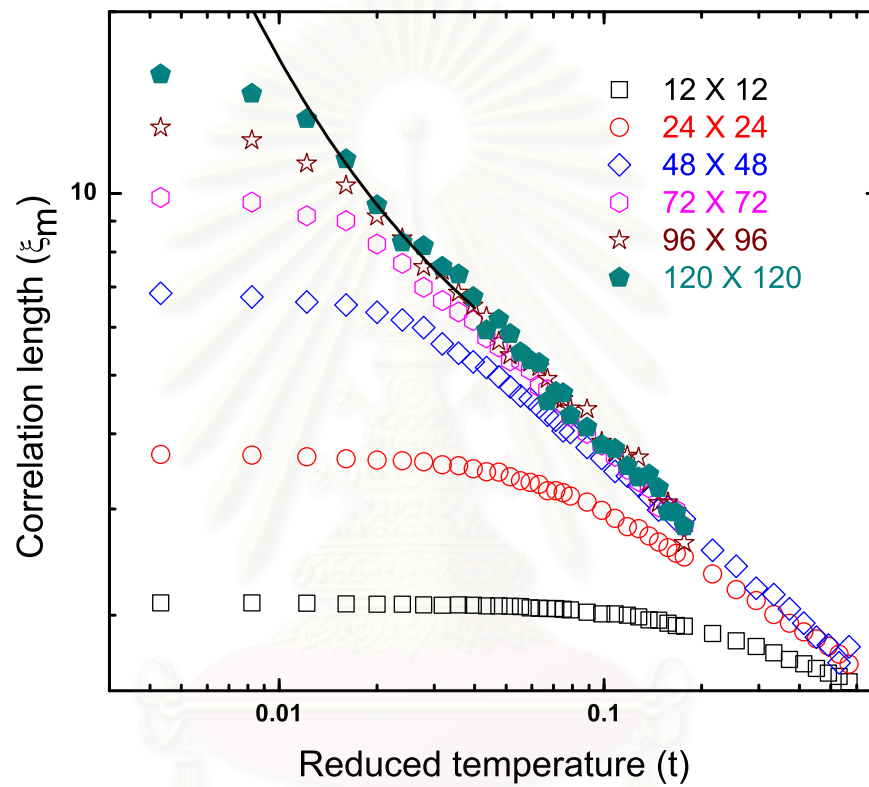


Figure 4.24: The correlation length ξ_m is plotted against the reduced temperature at different system sizes, the solid line denotes an exponential decay as $\xi_m = 2.50\exp(0.19t^{-1/2})$.

near the critical temperature, $t \leq 0.03$, marked by the solid line. This line is an exponential decay which can be written as $\xi_m = 2.50\exp(0.19t^{-1/2})$. This result is in good agreement with that value in Ref. (18).

4.8.2 The correlation length of chirality

In figure 4.25, the correlation length ξ_h is plotted against the temperature at different system sizes. Clearly, the correlation length increases when the temperature of the system approaches to the critical temperature. For small system sizes, $L \lesssim 24$, the correlation length increases slowly with decreasing the reduced temperature, while at the larger system sizes, the correlation length increases more faster than that of those sizes. The increasing of the correlation length occurs evidently near the critical temperature or at $t \rightarrow 0$. But at higher temperatures, $t \gtrsim 0.08$, the correlation length is slightly different except the correlation length of size $L = 12$. This increasing value of the correlation length near the critical temperature confirms that the correlation length diverges at the critical temperature for the infinite system size.

In order to know the behavior of the correlation length, we plot the correlation length against the reduced temperature at the different temperatures in the log–log scale as shown in figure 4.26. For the small system sizes, $L \leq 48$, the correlation length is observed in a wide range ($T = 0.514 - 0.800$). But for the larger system sizes, we observe the correlation length in a small range ($T = 0.514 - 0.600$) to save unnecessary time. We can see that the power law of the correlation length was found at high temperatures for small system sizes, for example, $t \gtrsim 0.2$ for $L = 12$. But near the critical temperature, the finite size effect prevents this behavior. At larger system sizes, the power law was found at lower temperatures. The dash line shows the logarithmic behavior of the correlation length of size $L = 120$. We estimate that the critical exponent $\nu = 0.74$. This value differs from the value of the Ising universality class, $\nu = 1$. However, the inconsistency was also found in those Ref. (5–7, 9, 12–15, 19, 22, 26, 27) which show that the

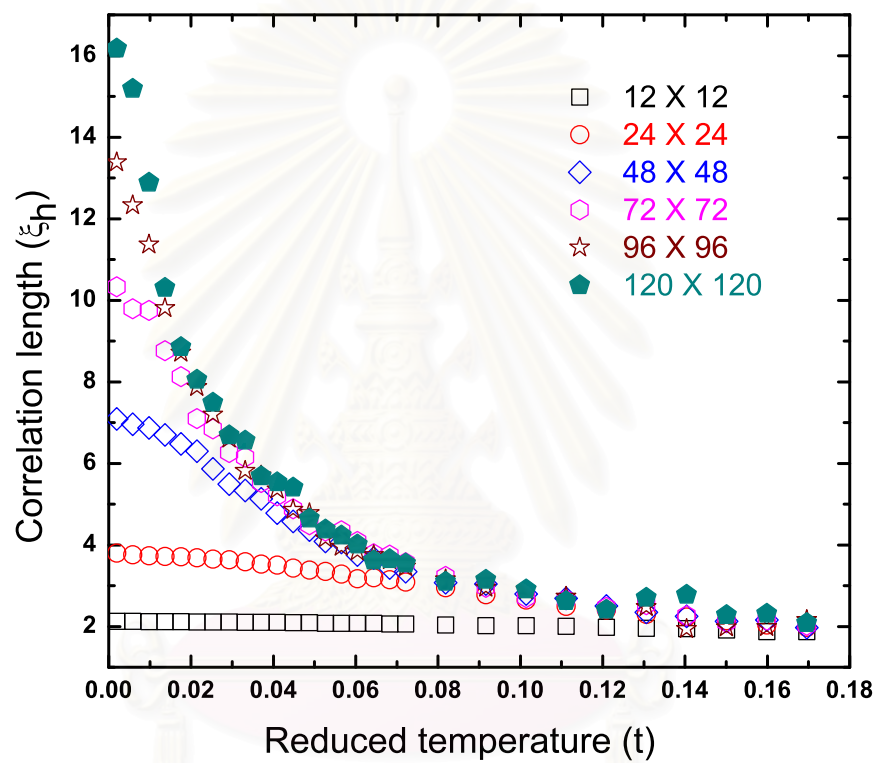


Figure 4.25: The correlation length ξ_h is plotted against the reduced temperature at different system sizes.

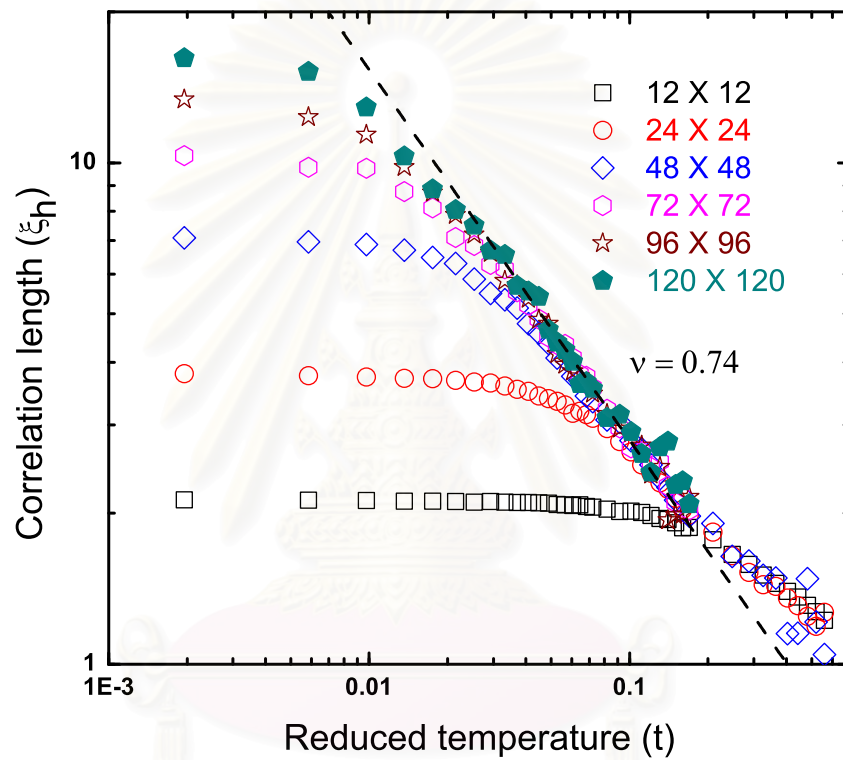


Figure 4.26: The correlation length ξ_h is plotted against the reduced temperature at different system sizes. The dash line has a slope = -0.74 .

critical exponent $\nu \approx 0.83$ rather than 1.

Next, the critical exponent ν of each system size is plotted against the inverted system size as shown in figure 4.27. The result shows that the critical exponent increases rapidly when the system size increases. It shows the strong finite size effect to the correlation length. However, we can see that the correlation length tends to the value, $\nu = 0.83$, which is marked by the dash line, rather than the Ising value. This result shows that the Ising-like transition may not belong to the Ising universality class.

The all results of the behavior of the parameters and the values of the critical exponents of this work compared to those results in Ref. (5, 14, 20, 22) are listed in Table 4.1 for the $U(1)$ symmetry and in Table 4.2 for the Z_2 symmetry.

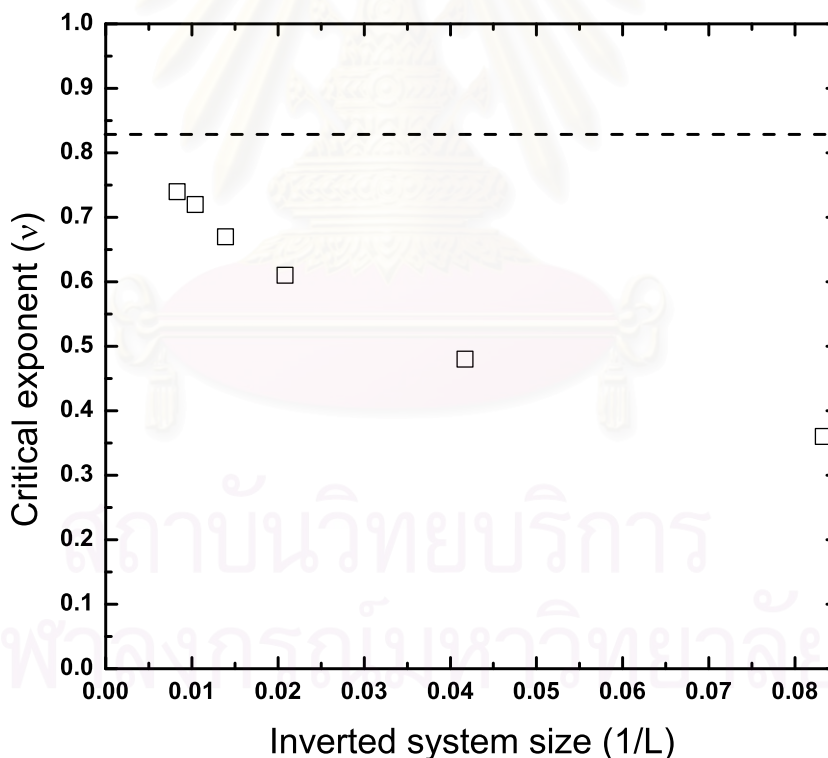


Figure 4.27: The system size dependence of ν is plotted against the inverted system size $1/L$. The dash line marks the value $\nu = 0.83$.

Table 4.1: The results of the parameters of the $U(1)$ symmetry on the triangular lattice.

Parameter	Exponent	This work	[5]	[14]	[22]
T_{KT}	—	0.509(8)	0.513(2)	0.508(1)	0.501(2)
$C_m(r) \sim \frac{1}{r^{\eta_{KT}}}$	η'_{KT} at $T = T_{KT}$	0.30	—	—	—
$\xi_m \sim \exp(a_0 t^{-1/2})$	—	2.50* $\exp(0.19t^{-1/2})$	—	—	—
$m_A \sim L^{-x}$	x	0.16	—	—	—

Table 4.2: The results of the parameters of the Z_2 symmetry on the triangular lattice.

Parameter	Exponent	This work	[5]	[14]	[20]	[22]
T_I	—	0.513(0)	0.513(2)	0.512(1)	—	0.513(1)
$C_h(r) \sim \frac{1}{r^{\eta_I}}$	η_I at $T = T_I$	0.19	—	0.250	—	0.25
$\xi_h \sim t ^{-\nu}$	ν	0.74	0.83	0.84	—	0.83
$c_{V_h} \sim t ^{-\alpha}$	α	0.45	—	—	—	0.33
$\chi_h \sim t ^{-\gamma}$	γ	1.05	—	—	1.73	1.45
$h \sim (-t)^\beta$	β	0.125	0.12	0.106	0.123	0.11

CHAPTER V

Conclusions

In this thesis, we have investigated phase transitions of the frustrated antiferromagnetic XY model on the triangular lattice via the simulation methods. Here, each chapter will be summarized and concluded as follows.

In the first chapter, we introduce the model of this study and related models which describe an array of Josephson junctions under an external magnetic field, discotic liquid crystals and the orientation ordering of CF_3Br monolayers physisorbed on graphite and then some inconsistencies of its behavior will be concerned.

In the second chapter, we illustrate a simple idea of the phase transition after that we provide more details about the model and the related theory of the thermodynamic parameters and other parameters.

In the third chapter, we describe the algorithm and the simulation techniques of this work.

In the fourth chapter, we show all simulation results of this study. Firstly, concerning to an equilibrium state of the system, we generate an equilibrium time by plotting the energy versus time in MCS steps. After the time, we assume the system is in the equilibrium state. Next section, the spin and the staggered chirality configurations at equilibrium states and at different system sizes are shown to illustrate the temperature dependence of the spins and the staggered chirality. Next result, we show clearly that the system has two separate transition temperatures, $T_{KT} < T_I$. These temperatures lie close to each other about 0.6% compared

with the lower temperature. The energy of the system smoothly decreases with decreasing the temperature and it has a signal of the second order phase transition around $T \approx 0.5$ due to its slope tends to infinity at this temperature. At lower temperatures, the energy approaches its minimum value at the ground state when the temperature goes to zero.

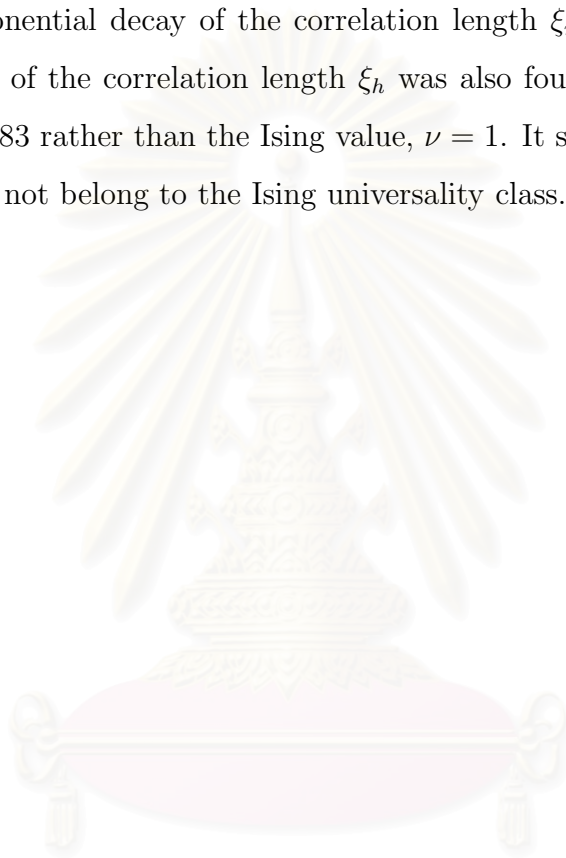
The system size dependence of the magnetization was found both at high temperatures and at low temperatures. It varies continuously from high temperature disordered states with the zero magnetization to lower temperature ordered states with a finite magnetization through the critical temperature. We also found that the magnetization has a power law $m_A \sim L^{-x}$ at $T \leq T_{KT}$ with the exponent $x = 0.16$ at $T = T_{KT}$. It differs from the value $x = 1/8$ of the KT transition and we think that the temperature may affect the result. As the same result except at low temperatures, at which the staggered chirality has a power law, $h \sim (-t)^\beta$ with $\beta = 0.125$. This value is in good agreement with the exact value $\beta = 1/8$ of the Ising transition.

The results show that the specific heat has a finite value both at high and low temperatures but tends to infinity at the critical temperatures. Two interpretations of scaling forms are used, first we assume the specific heat has a power law $c_V \sim |t|^{-\alpha}$ and we estimate that $\alpha = 0.45$ which confirms the non-logarithmic behavior of the specific heat. For the another interpretation, we found that the peak c_{V_*} of the specific heat changes from the power law behavior $c_{V_*} \sim L^{\alpha/\nu}$ with $\alpha/\nu = 0.52$ at $L \leq 48$ to the logarithmic behavior $c_{V_*} \sim \log(L)$ with $\alpha/\nu = 0$ at $L > 48$. The inconsistency of two interpretations was found at $L > 48$ and we think that for $L > 48$, our simulations can not separate the peaks of the specific heat out so we have not confirmed the logarithmic behavior at those sizes.

Next result, the magnetic susceptibility was found a finite value at high temperatures and it becomes infinity at the critical temperatures and at low temperatures as $L \rightarrow \infty$. Above T_I , the magnetic susceptibility decays as a power law as $\chi \sim |t|^{-\gamma}$ with $\gamma = 1.05$ near T_I and $\gamma = 1.23$ at higher temperatures. The correlation functions decrease with increasing the distance. The power law of the

correlation functions was found at the critical temperatures with $\eta_{KT} = 0.30$ and $\eta_I = 0.19$ which differ from the expected value $\eta_{KT} = \eta_I = 0.25$ because of the size dependence of the exponents.

Finally, the correlation lengths increase with decreasing the reduced temperature from high temperatures to the critical temperatures. The correlation lengths tend to infinity at the critical temperatures with increasing the system size. We found the exponential decay of the correlation length ξ_m near T_{KT} for $L \geq 96$. The power law of the correlation length ξ_h was also found with $\nu = 0.74$ and it tends to $\nu = 0.83$ rather than the Ising value, $\nu = 1$. It seems that the Ising-like transition may not belong to the Ising universality class.



สถาบันวิทยบริการ
จุฬาลงกรณ์มหาวิทยาลัย

References

- [1] Villain, J. Two-level systems in a spin-glass model: I. General formalism and two-dimensional model. *J. Phys. C* **10** (1977): 4793–4803.
- [2] Teitel, S., and Jayaprakash, C. Phase transitions in frustrated two-dimensional XY models. *Phys. Rev. B* **27** (1983): 598–601.
- [3] Choi, M. Y., and Stroud, D. Critical behavior of pure and diluted XY models with uniform frustrations. *Phys. Rev. B* **32** (1985): 5773–5775.
- [4] Berge, B., Diep, H. T., Ghazali, A., and Lallemand, P. Phase transitions in two-dimensional uniformly frustrated XY spin systems. *Phys. Rev. B* **34** (1986): 3177–3184.
- [5] Lee, J., Kosterlitz, J. M., and Granato, E. Monte Carlo study of frustrated XY models on a triangular and square lattice. *Phys. Rev. B* **43** (1991): 11531–11534.
- [6] Lee, S., and Lee, K. -C. Phase transitions in the fully frustrated XY model studied with use of the microcanonical Monte Carlo technique. *Phys. Rev. B* **49** (1994): 15184–15189.
- [7] Granato, E., and Nightingale, M. P. Chiral exponents of the square-lattice frustrated XY model: A Monte Carlo transfer-matrix calculation. *Phys. Rev. B* **48** (1993): 7438–7444.
- [8] Knops, Y. M. M., Nienhuis, B., Knops, H. J. F., and Blöte, H. W. J. 19-vertex version of the fully frustrated XY model. *Phys. Rev. B* **50** (1994): 1061–1073.
- [9] Ramirez-Santiago, G., and José, J. V. Critical exponents of the fully frustrated two-dimensional XY model. *Phys. Rev. B* **49** (1994): 9567–9582.

- [10] Olsson, P. Two phase transitions in the fully frustrated XY model. *Phys. Rev. Lett.* **75** (1995): 2758–2761.
- [11] Jeon, G. S., Park, S. Y., and Choi, M. Y. Double transitions in the fully frustrated XY model. *Phys. Rev. B* **55** (1997): 14088–14091.
- [12] Luo, H. J., Schülke, L., and Zheng, B. Dynamic approach to the fully frustrated XY model. *Phys. Rev. Lett.* **81** (1998): 180–183.
- [13] Boubcheur, E. H., and Diep, H. T. Critical behavior of the two–dimensional fully frustrated XY model. *Phys. Rev. B* **58** (1998): 5163–5165.
- [14] Ozeki, Y., and Ito, N. Nonequilibrium relaxation analysis of fully frustrated XY models in two dimensions. *Phys. Rev. B* **68** (2003): 054414.
- [15] Minnhagen, P., Kim, B. J., Bernhardsson, S., and Cristofano, G. Phase diagram of generalized fully frustrated XY model in two dimensions. *Phys. Rev. B* **76** (2007): 224403.
- [16] Resnick, D. J., Garland, J. C., Boyd, J. T., Shoemaker, S., and Newrock, R. S. Kosterlitz–Thouless transition in proximity–coupled superconducting arrays. *Phys. Rev. Lett.* **47** (1981): 1542–1545.
- [17] Hébert, M., and Caillé, A. Mean–field phase diagram of a coupled XY –Ising model for discotic liquid crystals. *Phys. Rev. E* **51** (1995): R1651–R1654.
- [18] Noh, J. D., Rieger, H., Enderle, M., and Knorr, K. Critical behavior of the frustrated antiferromagnetic six–state clock model on a triangular lattice. *Phys. Rev. E* **66** (2002): 026111.
- [19] Surungan, T., Okabe, Y., and Tomita, Y. Study of the fully frustrated clock model using the Wang–Landau algorithm. *J. Phys. A* **37** (2004): 4219–4230.
- [20] Lee, D. H., Joannopoulos, J. D., Negele, J. W., and Landau, D. P. Discrete–symmetry breaking and novel critical phenomena in an anti-

- ferromagnetic planar (XY) model in two dimensions. *Phys. Rev. Lett.* **52** (1984): 433–436.
- [21] Himbergen, J. E. V. Monte Carlo study of a generalized–planar–model antiferromagnet with frustration. *Phys. Rev. B* **33** (1986): 7857–7860.
- [22] Lee, S., and Lee, K. –C. Phase transitions in the fully frustrated triangular XY model. *Phys. Rev. B* **57** (1998): 8472–8477.
- [23] Nho, K., and Landau, D. P. Spin–dynamics simulations of the triangular antiferromagnetic XY model. *Phys. Rev. B* **66** (2002): 174403.
- [24] José, J. V., Kadanoff, L. P., Kirkpatrick, S., and Nelson, D. R. Renormalization, vortices, and symmetry–breaking perturbations in the two–dimensional planar model. *Phys. Rev. B* **16** (1977): 1217–1241.
- [25] Kosterlitz, J. M. The critical properties of the two–dimensional xy model. *J. Phys. C* **7** (1974): 1046–1060.
- [26] Granato, E., Kosterlitz, J. M., Lee, L., and Nightingale, M. P. Phase transitions in coupled XY –Ising systems. *Phys. Rev. Lett.* **66** (1991): 1090–1093.
- [27] Lee, J. –R. Phase transitions in the two–dimensional classical lattice Coulomb gas of half–integer charges. *Phys. Rev. B* **49** (1994): 3317–3321.
- [28] Grest, G. S. Critical behavior of the two–dimensional uniformly frustrated charged Coulomb gas. *Phys. Rev. B* **39** (1989): 9267–9272.
- [29] Yeomans, J. M. *Statistical mechanics of phase transitions*. Oxford: Clarendon Press, 1992.
- [30] Huang, K. *Statistical mechanics*. New York: John Wiley & Sons, 1987.
- [31] Landau, D. P., and Binder, K. *A guide to Monte Carlo simulations in statistical physics*. Cambridge: Cambridge University Press, 2000.

- [32] Bellac, M. L. *Quantum and statistical field theory*. Oxford: Clarendon Press, 1991.
- [33] Press, W. H., Teukolsky, S. A., Vetterling, W. T., and Flannery, B. P. *Numerical recipes in C: the art of scientific computing*. Cambridge: Cambridge University Press, 1992.
- [34] Challa, M. S. S., and Landau, D. P. Critical behavior of the six–state clock model in two dimensions. *Phys. Rev. B* **33** (1986): 437–443.
- [35] Tsai, S. –H., and Salinas, S. R. Fourth–order cumulants to characterize the phase transitions of a spin–1 Ising model. *Braz. J. Phys.* **28** (1998): 58–65.
- [36] Isihara, A. Magnetic exchange energy of two–dimensional electrons. *Z. Phys. B* **73** (1988): 15–16.



สถาบันวิทยบริการ
จุฬาลงกรณ์มหาวิทยาลัย



APPENDICES

สถาบันวิทยบริการ
จุฬาลงกรณ์มหาวิทยาลัย

Appendix A

Finite Size Scaling

For the infinite system is near the critical temperature, a thermodynamic parameter can be usually written as Eq. (2.1), for example, the magnetic susceptibility is written as

$$\chi \sim t^{-\gamma} \sim \xi^{\gamma/\nu}, \quad (\text{A.1})$$

where $\xi \sim t^{-\nu}$ is the correlation length. The correlation length and the magnetic susceptibility diverge at the critical temperature. But for a finite system size (L), this condition is only true at some temperatures in which the system size is greater than the correlation length, $L \gg \xi$. At the critical temperature, $L \ll \xi$, the correlation length never reaches to infinity and it will be cut off at some value depending on L , so χ can be written as $\chi \sim L^{\gamma/\nu}$. Eq. (A.1) may be written as a function of L/ξ as

$$\chi = L^{\gamma/\nu} \chi_0(L/\xi). \quad (\text{A.2})$$

The behavior of $\chi_0(L/\xi)$ must be followed

$$\chi_0(L/\xi) = \text{constant} ; \quad L \ll \xi, \quad (\text{A.3})$$

$$\chi_0(L/\xi) \sim (L/\xi)^{-\gamma/\nu} ; \quad L \gg \xi. \quad (\text{A.4})$$

Because of $L/\xi \propto Lt^\nu$ one can choose $L^{1/\nu}t$, then Eq. (A.2) is written as

$$\chi = L^{\gamma/\nu} \chi_0(L^{1/\nu}t). \quad (\text{A.5})$$

The other parameters can be written in the same manner as

$$m = L^{-\beta/\nu} m_0(L^{1/\nu}t), \quad (\text{A.6})$$

$$c_V = L^{\alpha/\nu} c_0(L^{1/\nu}t), \quad (\text{A.7})$$

where m and c_V are the magnetization and the specific heat, respectively.

Appendix B

Cumulants

The generating function $Z(j)$ of a probability distribution $P(\varphi)$ can be written as

$$Z(j) = Z(0) \sum_{n=0}^{\infty} \frac{j^n}{n!} \langle \varphi^n \rangle. \quad (\text{B.1})$$

$Z(j)$ can be written as a function of some parameter $W(j)$ which is analogous to a free energy, $Z(j) = Z(0)\exp[W(j)]$ or $W(j) = \ln[Z(j)/Z(0)]$. The cumulants of order n , $\langle \varphi^n \rangle_c$, can be defined by [32]

$$W(j) = \sum_{n=1}^{\infty} \frac{j^n}{n!} \langle \varphi^n \rangle_c, \\ \langle \varphi^n \rangle_c = \left. \frac{\partial^n W(j)}{\partial j^n} \right|_{j=0}. \quad (\text{B.2})$$

Let

$$x(j) = \frac{Z(j)}{Z(0)} = \sum_{n=0}^{\infty} \frac{j^n}{n!} \langle \varphi^n \rangle = \exp[W(j)].$$

One can find that

$$\begin{aligned} \frac{\partial x(j)}{\partial j} &= x(j) \frac{\partial W(j)}{\partial j}, \\ \frac{\partial^2 x(j)}{\partial j^2} &= x(j) \frac{\partial^2 W(j)}{\partial j^2} + x(j) \left(\frac{\partial W(j)}{\partial j} \right)^2, \\ \frac{\partial^3 x(j)}{\partial j^3} &= x(j) \frac{\partial^3 W(j)}{\partial j^3} + 3x(j) \frac{\partial^2 W(j)}{\partial j^2} \frac{\partial W(j)}{\partial j} + x(j) \left(\frac{\partial W(j)}{\partial j} \right)^3, \\ \frac{\partial^4 x(j)}{\partial j^4} &= x(j) \frac{\partial^4 W(j)}{\partial j^4} + 4x(j) \frac{\partial^3 W(j)}{\partial j^3} \frac{\partial W(j)}{\partial j} + 3x(j) \left(\frac{\partial^2 W(j)}{\partial j^2} \right)^2 \\ &\quad + 6x(j) \frac{\partial^2 W(j)}{\partial j^2} \left(\frac{\partial W(j)}{\partial j} \right)^2 + x(j) \left(\frac{\partial W(j)}{\partial j} \right)^4. \end{aligned} \quad (\text{B.3})$$

From Eq. (B.2) and Eq. (B.3) the cumulant of each order can be written as

$$\begin{aligned} \langle \varphi \rangle_c &= \langle \varphi \rangle, \\ \langle \varphi^2 \rangle_c &= \langle \varphi^2 \rangle - \langle \varphi \rangle_c^2 = \langle (\varphi - \langle \varphi \rangle)^2 \rangle, \end{aligned}$$

$$\begin{aligned}
\langle \varphi^3 \rangle_c &= \langle \varphi^3 \rangle - 3\langle \varphi^2 \rangle_c \langle \varphi \rangle_c - \langle \varphi \rangle_c^3 = \langle (\varphi - \langle \varphi \rangle)^3 \rangle, \\
\langle \varphi^4 \rangle_c &= \langle \varphi^4 \rangle - 4\langle \varphi^3 \rangle_c \langle \varphi \rangle_c - 3\langle \varphi^2 \rangle_c^2 - 6\langle \varphi \rangle_c^2 \langle \varphi^2 \rangle_c - \langle \varphi \rangle_c^4 \\
&= \langle (\varphi - \langle \varphi \rangle)^4 \rangle - 3\langle (\varphi - \langle \varphi \rangle)^2 \rangle^2.
\end{aligned} \tag{B.4}$$

The fourth-order cumulant $\langle \varphi^4 \rangle_c$ is more often written as

$$U_4 = 1 - \frac{\langle (\varphi - \langle \varphi \rangle)^4 \rangle}{3\langle (\varphi - \langle \varphi \rangle)^2 \rangle^2}. \tag{B.5}$$

This equation is also called ‘the Binder cumulant.’

Consider the magnetization m , the probability distribution function of the magnetization $p(m)$ is written as [35]

$$p(m) = \frac{1}{2}C \exp \left[-\frac{(m + m_0)^2}{2\sigma^2} \right] + \frac{1}{2}C \exp \left[-\frac{(m - m_0)^2}{2\sigma^2} \right], \tag{B.6}$$

where $C = (2\pi\sigma^2)^{-1/2}$ is a normalization factor and $\sigma \propto L^{-2}$. The $p(m)$ has a single peak at $m_0 = 0$ at high temperatures and two peaks at $\pm|m_0|$ at low temperatures. As the $p(m)$ is symmetric, then $\langle m^n \rangle = 0$ for odd n . So for a finite system size the Binder cumulant of the magnetization can be written as

$$U_4(L) = 1 - \frac{\langle m^4 \rangle}{3\langle m^2 \rangle^2}. \tag{B.7}$$

For $n = 2$ and 4 , $\langle m^2 \rangle$ and $\langle m^4 \rangle$ can be calculated by

$$\begin{aligned}
\langle m^2 \rangle &= \int_{-\infty}^{\infty} m^2 p(m) dm = \sigma^2 + m_0^2, \\
\langle m^4 \rangle &= \int_{-\infty}^{\infty} m^4 p(m) dm = 3\sigma^4 + 6\sigma^2 m_0^2 + m_0^4.
\end{aligned} \tag{B.8}$$

Then the Binder cumulant is given by

$$U_4(L) = 1 - \frac{3\sigma^4 + 6\sigma^2 m_0^2 + m_0^4}{3(\sigma^2 + m_0^2)^2}. \tag{B.9}$$

At high temperatures ($m_0 = 0$), we can see that $U_4 = 0$. At low temperatures and $L \rightarrow \infty$ ($\sigma \rightarrow 0$), $U_4 \rightarrow 2/3$. At the critical temperature ($Lt^{1/\nu} = 0$), by using Eq. (A.6) and Eq. (B.7) we can find that the Binder cumulant is independent of L as

$$U_4 = 1 - \frac{\langle m_0^4(0) \rangle}{3\langle m_0^2(0) \rangle^2} \equiv U^*, \tag{B.10}$$

where U^* is a fixed point [31].

Vitae

Manit Klawtanong was born on June 16, 1983 in Songkhla, Thailand. He received Bachelor's Degree of Science in Physics from Prince of Songkla University in 2006.

CONFERENCE PRESENTATIONS:

- 2009 M. Klawtanong and C. Srinitiwawong. Two-Separate Critical Temperatures of the Frustrated Antiferromagnetic ($FAXY$) XY Model on the Triangular Lattice. The 12nd National Graduate Research Conference, Khon Kaen University (12–13 February; 2009)
- 2009 M. Klawtanong and C. Srinitiwawong. Phase Transitions in the Frustrated Antiferromagnetic XY Model on the Triangular Lattice. Siam Physics Congress 2009, Phetchburi, Thailand (19–21 March; 2009)



สถาบันวิทยบริการ
จุฬาลงกรณ์มหาวิทยาลัย